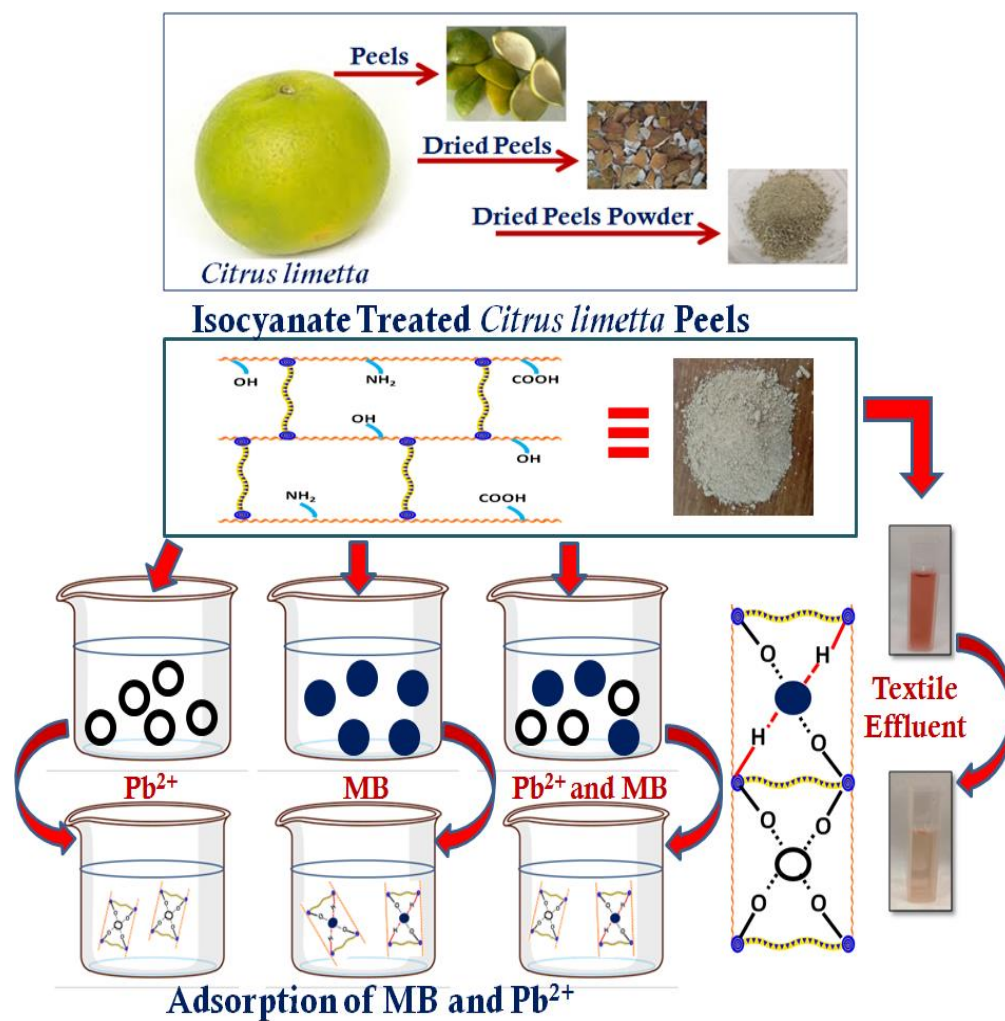


Chapter V (B)

Citrus limetta derived eco-friendly bioadsorbent for efficient elimination of organic dyes and heavy metal ions



5.2.1. Introduction

Water is an essential source for all living organisms to survive. In current scenario, the increasing pollution loads on aquatic system are of significant concern. The discharge of wastewater effluents from agricultural, residential and industrial resources introduces various organic and inorganic pollutants such as pesticides, heavy metals, cyanides, hydrocarbon solvents, dyes, etc. into natural systems¹. Along with these, wastes generated from industries viz. leather, steel, electroplating, metal foundry and battery manufacturing industries are potential source of pollutants. Coloured wastewater resulting from dye processing has negative impacts on dominant plants, animals as well as the ecosystem. Besides being the annoying aesthetic nature of wastewater dye they also affect the food web of the ecosystem and finally affect humans negatively². Another major environmental issue is heavy metals, which pose a significant risk because of their persistent nature and tendency to bioaccumulate. Trace amounts of heavy metals and dyes in the water are undesirable and harmful because they are carcinogenic, mutagenic and toxic. Methylene Blue (MB), an organic dye have tendency to cause sore throat, skin irritation, asthma, eye irritation etc. whereas, Lead (Pb), is a hypertoxic heavy metal causes damage of liver, kidney as well as disorders of central nervous system³. Lead is one of the non-destructive heavy metal that binds with other biomolecules and transformed into different chemical form in living organisms⁴. Therefore, the greatest need of their treatment prior to discharging into the natural environment is necessary. Heavy metals influence the biochemical and physiological procedures that can be poisonous for macro-organism and micro-organisms reducing growth, preventing photosynthesis, and deteriorating cell organelles⁵.

In order to eliminate dyes and heavy metals from contaminated water various chemical, physical and biological techniques have been reported so far. Some of the methods among them are ion exchange, adsorption, ozonation, oxidative processes and membrane process. Adsorption method is one of the effective technique in terms of cost-effectiveness and convenience to eliminate heavy metals and dyes for wastewater⁶. Number of adsorbents has been reported till date to remove pollutants from contaminated water. Some of them are agricultural wastes⁷, alumina⁸, graphene oxide⁹, hydrogels^{10,11}, aerogels^{12,13}, mesoporous SiO₂¹⁴, MCM-41 and MCA¹⁵, activated carbon¹⁶, aerogels^{12,13}, polymer-clay¹⁷, nanoadsorbent¹⁸, bioadsorbents etc.¹⁹

Currently the major attention of researchers has been focused on bioadsorbents for wastewater remediation process. They exhibit high sorption capacity, easy availability, regeneration, less

financial input, modest sludge generation, non-toxic and eco-friendly nature in comparison to other expensive methods²⁰. The existence of several functional groups like $-NH_2$, $-COOH$, and $-OH$ on bioadsorbent surface helps in pollutants adsorption²¹. Several bioadsorbent based pollutant removal studies have been reported. Taro (*Colocasiaes-culenta*(L.) Schott) has been used for elimination of lead from aqueous solution has been reported utilizing.²² According to the study of Han et al., lead ions adsorption from aqueous solution has been reported using native wheat straw biomass and further modifying into biochar and ball-milled biochar showing maximum adsorption capacity of 46.33, 119.55 and 134.68 mg/g²³. Report of Lima et al., demonstrated the removal of methylene blue dye using bioadsorbent *Enterolobium contortisiliquum* with 79% removal efficiency²⁴. Since simultaneous adsorption of organic and inorganic pollutants are of great importance for treatment of wastewater and only few studies have been reported in this context. Therefore, this study reports single and binary component system adsorption of organic dye and heavy metal.

In this study, we report a simple, facile and superficial method to synthesize *Citrus limetta* based bioadsorbent modified with cross-linker hexamethylene diisocyanate (HMDI). The synthesized modified *Citrus limetta* (MCL) bioadsorbent has been successfully used for organic and inorganic pollutants removal from aqueous solution within few hours of application. The formation of urethane linkage due to HMDI with native *Citrus limetta* surface results stable bioadsorbent system with various active sites. The synthesized bioadsorbent was characterized using different methods like Fourier Transform Infrared Spectroscopy (FTIR), Thermogravimetric Analysis (TGA), Scanning Electron Microscope (SEM), Brunauer-Emmett-Teller (BET), X-ray Diffraction (XRD), Energy dispersive X-ray (EDX) etc. have been used for characterization of synthesized bioadsorbent. All adsorption parameters like dosage, concentration, temperature, pH variations have been studied in detail. Experimental data fitted well on thermodynamic, kinetics and isotherm models. MCL bioadsorbent was successfully used to eliminate dye and heavy metal from aqueous solution as well as color from environmental sample. This adsorbent system could be utilized as a promising approach in contaminated water treatment.

5.2.2. Materials and Methods

5.2.2.1. Materials

Hexamethylene diisocyanate (HMDI), dibutyltin dilaurate (DBTDL) and Acetone were purchased from Sigma Aldrich, India. N, N Dimethylformamide (DMF) was purchased from Qualigens, Bombay, India. Methylene Blue and Lead Nitrate were obtained from Fisher Scientific, Navi Mumbai, India. The *Citrus limetta* peel has been collected from fruit market, Vadodara. Analytical grade reagents were used as received. The solutions of dye were prepared using de-ionized water.

5.2.2.2. Synthesis of Modified *Citrus limetta* (MCL)

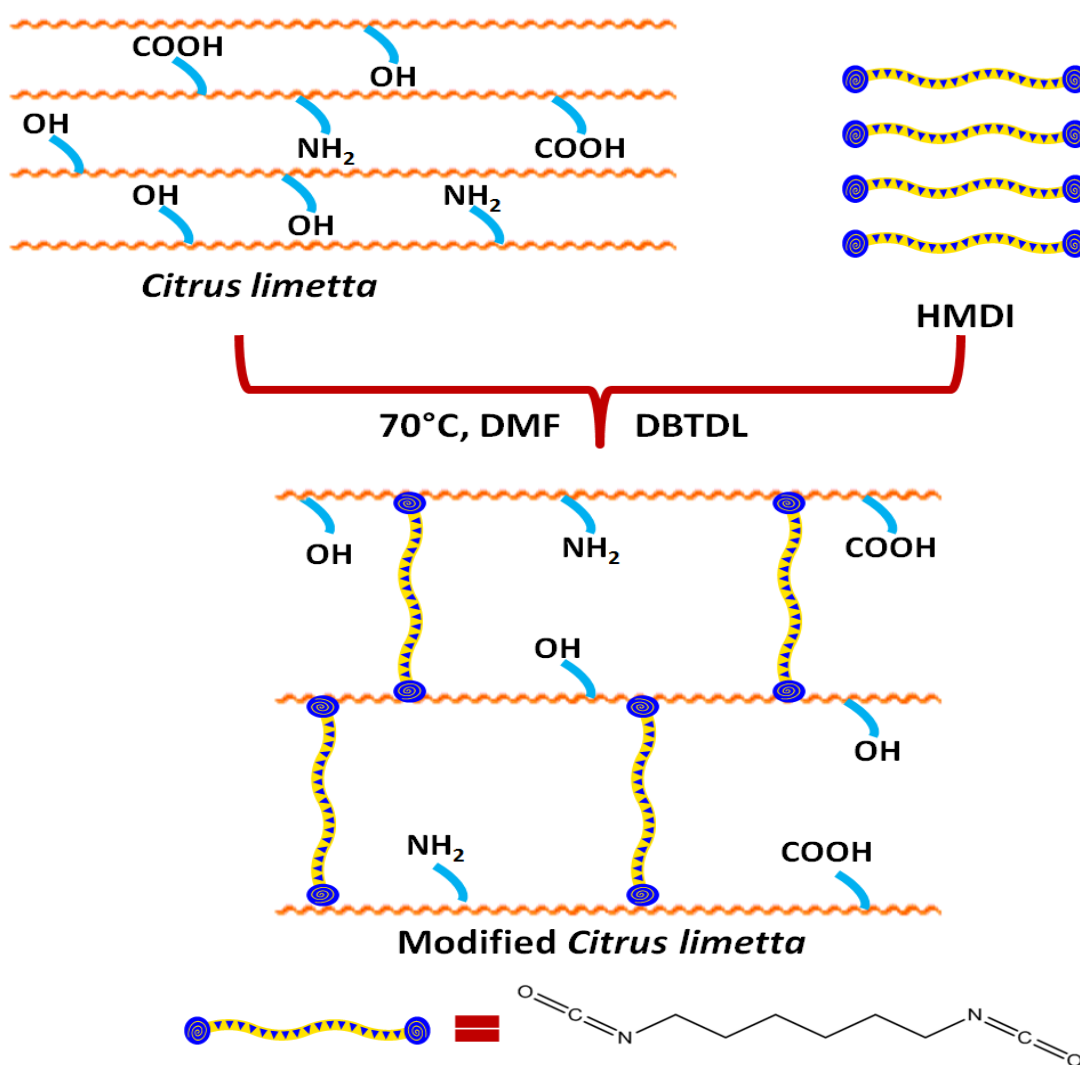


Figure 5.2.1: Synthetic scheme of MCL

For the synthesis of CLM, *Citrus limetta* peels have been collected and washed thoroughly. Peels have been cut into small pieces and dehydrated in oven at 100 °C for 5-6 hours. After drying, peels have been crushed and converted into uniform size of *Citrus limetta*. 100 mg powder of *Citrus limetta* was dispersed in DMF (5-8 ml) on stirrer under nitrogen atmosphere. 100 μ L HMDI was dissolved into 1 mL of DMF and added into reaction mixture dropwise under constant stirring. The obtained reaction mixture was heated at a constant temperature of 70°C in oil bath in the presence of catalyst DBTDL (50 μ L) for 1 hour in a round bottom flask. The system was allowed to stir continuously to complete the synthesis. The synthesized MCL was separated by filtration and cleaned with water and acetone. The product was dried and stored under vacuum for further use in experiments. The synthetic scheme has been represented in **Figure 5.2.1**.

5.2.2.3. Characterization of MCL

PerkinElmer IR spectrophotometer was used to record FTIR spectra of MCL as KBr discs at room temperature. Energy Dispersive Spectrometer (EDS) analysis of the vacuum dried MCL was recorded by the model-JSM-5610 LV. The Surface area and porosity of SPNA were measured using a volumetric adsorption system (Micromeritics Instrument corporation, USA, model ASAP 2020) using N₂ adsorption/desorption isotherms at 77 K up to 1 bar. Before measurements, the samples were activated (degassed) by heating at the rate of 1 K min⁻¹ up to 295 K under vacuum. Surface area was calculated using the Brunauer– Emmet–Teller (BET) method and the porosity by the Barrett– Joyner–Halenda (BJH) method. Thermo gravimetric analysis (TGA) was performed using TG–DTA 6300 INCARP EXSTAR 6000 at a heating rate of 10°C/min in the temperature range of 30–500°C with nitrogen atmosphere maintained throughout the measurement. The structure of the hydrogel was investigated using a D2 Phase 2 Bruker X-ray powder diffractometer at room temperature. X-rays of wavelength 0.1454 nm (Cu K-alpha) were produced using a tube, a dried and pressed powder of the material was used as a sample and diffraction patterns were collected in 0.05 steps per second with 2 θ ranging between 5° and 80°. UV-vis spectrophotometric measurements were done on Cary 60 UV-vis spectrophotometer (Agilent Technologies). PinAAcle 500 Atomic Absorption Spectrometer of Perkin Elmer has been used for heavy metal determination.

5.2.2.4. Adsorption of organic and inorganic pollutants

To evaluate the adsorption capacity of MCL, one organic pollutant i.e. Methylene Blue (MB) dye and one inorganic pollutant i.e. heavy metal Lead (Pb^{2+}) were used as models for adsorption studies. The adsorption process was carried out in 150 mL conical flasks containing 50 mL of model solutions. In order to determine the optimum quantity of MCL to be used in subsequent experiments, different amount (25- 200 mg) of MCL was added in 100 mg/L of prepared MB and Pb^{2+} solutions individually. The solutions were placed on magnetic stirring for different time intervals; aliquots were collected and further measurement was carried out for determination of unadsorbed pollutant content using UV-Vis Spectrophotometer and Atomic Absorption Spectrometer. For determination of optimum concentration of MB and Pb^{2+} to be used in successive experiments, different concentrations (50 – 250 mg/L) of dye and heavy metal were prepared and optimum amount of MCL was added to the solutions. All the solutions were placed on shaker for 7 hours at 35°C (other than temperature variation study) and shaking speed of 160 rpm to attain equilibrium condition. Supernatant was separated and analyzed using UV-visible spectrophotometer at the wavelength range of 400-800 nm and Atomic Absorption Spectrometer. For pH variation study, 50 mL of 100 mg/L MB and Pb^{2+} were taken with 100mg MCL at different pH (2-12) and kept on shaker for equilibrium study, supernatants were collected after adsorption and analyzed using UV-visible spectrophotometer ($\lambda_{\text{max}} = 665$ for MB) and Atomic Absorption Spectrometer. The pH adjustments were done using NaOH and HCl solutions. For determination of point zero charge (pH_{PZC}), 50 mL pH 2-10 solutions were continuously stirred with 50 mg MCL and final pH of solutions were measured. The graph between ΔpH (difference between initial and final pH value) and initial pH demonstrate pH_{PZC} ²⁵. Using the above optimized conditions, kinetics experiments were executed at various time intervals. The effect of temperature on adsorption has also been studied on different temperature from 35°C to 55°C. Each experiment has been performed in triplicates and mean values were reported. The adsorption capacity, removal percentage and adsorption at particular time ‘*t*’ were calculated using the following equations²⁶:

$$q_e = \frac{(C_0 - C_e)}{m} * V \dots\dots\dots (1)$$

$$\%R_e = \frac{C_0 - C_e}{C_e} * 100 \dots\dots\dots (2)$$

$$q_t = \frac{(C_0 - C_t)}{m} * V \dots\dots\dots (3)$$

where, q_e denotes adsorption capacity (mg/g), q_t is adsorption capacity at particular time 't' (mg/g) and %*Re* denotes removal efficiency of pollutants; C_0 represents initial concentration (mg/L), C_e is equilibrium concentration (mg/L) and C_t denotes the concentration at time 't' (mg/L) of pollutants in aqueous solution; 'V' represents the volume of solution (L) and 'm' denotes the weight of the adsorbent (g).

5.2.2.5. Simultaneous Adsorption of MB and Pb²⁺

Binary system of MB and Pb²⁺ was used for adsorption study simultaneously owing to practical relevance. For this study, 50 mL of 50 mg/L MB and 50 mg/L Pb²⁺ solution were prepared and ratio of mixing was 1:1. The adsorption study was performed till equilibrium and supernatant were observed under UV-visible spectrophotometer and Atomic Absorption Spectrometer.

5.2.2.6. Desorption Experiment and Reusability

MCL (100 mg) was placed in conical flask containing 100 mg/L MB and 100 mg/L Pb²⁺ individually and the solutions were magnetically stirred for 7 hours. After adsorption, supernatants were separated and final concentrations of dye and heavy metal ions were determined. The pollutant loaded MCL was desorbed by constant stirring with 0.1M HCl, the desorbed bioadsorbent were washed several times by distilled water, air dried and stored to reuse in new adsorption batch. The regenerated adsorbent was utilized in adsorption-desorption experiments upto five cycles. The desorption efficiency was calculated by using equation (4)²⁷.

$$\text{Desorption Efficiency} = \frac{\text{Amount of Pollutant Desorbed}}{\text{Amount of Pollutant Adsorbed}} \times 100 \dots\dots (4)$$

5.2.3. Results and Discussion

5.2.3.1. Characterization of Bioadsorbent

5.2.3.1.1. FTIR Spectra Analysis

The IR spectra for MCL, MCL+MB and MCL+Pb²⁺ (**Figure 5.2.2**) shows –OH stretching vibrations at 3335 cm⁻¹. The peaks in the range of 1500-1650 cm⁻¹ represents the stretching vibrations of carboxyl groups (-COOH). Peak at 2933, 2856 and 1576 shows stretching vibration of –NH, –CH and C=O groups corresponding the urethane linkage^{25,28}. The characteristic peaks at 1439, 1372, 1160, 1075 and 896 cm⁻¹ shows typical cellulose molecules bands⁶. The peaks in

the range of $1320\text{--}1210\text{ cm}^{-1}$ represents the appearance of --C--O and --C--H group²⁹. The FTIR spectrum of MCL represents significant number of functional groups for binding with adsorbate molecules. The peaks at 1075 and 1160 cm^{-1} is related with C-O-C stretching vibration representing polysaccharide skeleton of cellulose³⁰. Changes in intensity and shifting of peak position represent the adsorption of MB and Pb^{2+} on surface of MCL. The shifting of peak from 1626 to 1624 cm^{-1} (MB) and 1623 cm^{-1} (Pb^{2+}) signifies C=O/C=C bond involvement in the process of adsorption³¹. The band at 2933 cm^{-1} corresponds to antisymmetric and symmetric stretching of C–H bond associated with methyl and methylene groups. The decrease in intensity of hydroxyl and carboxyl groups represents their involvement in binding with organic and inorganic pollutant.

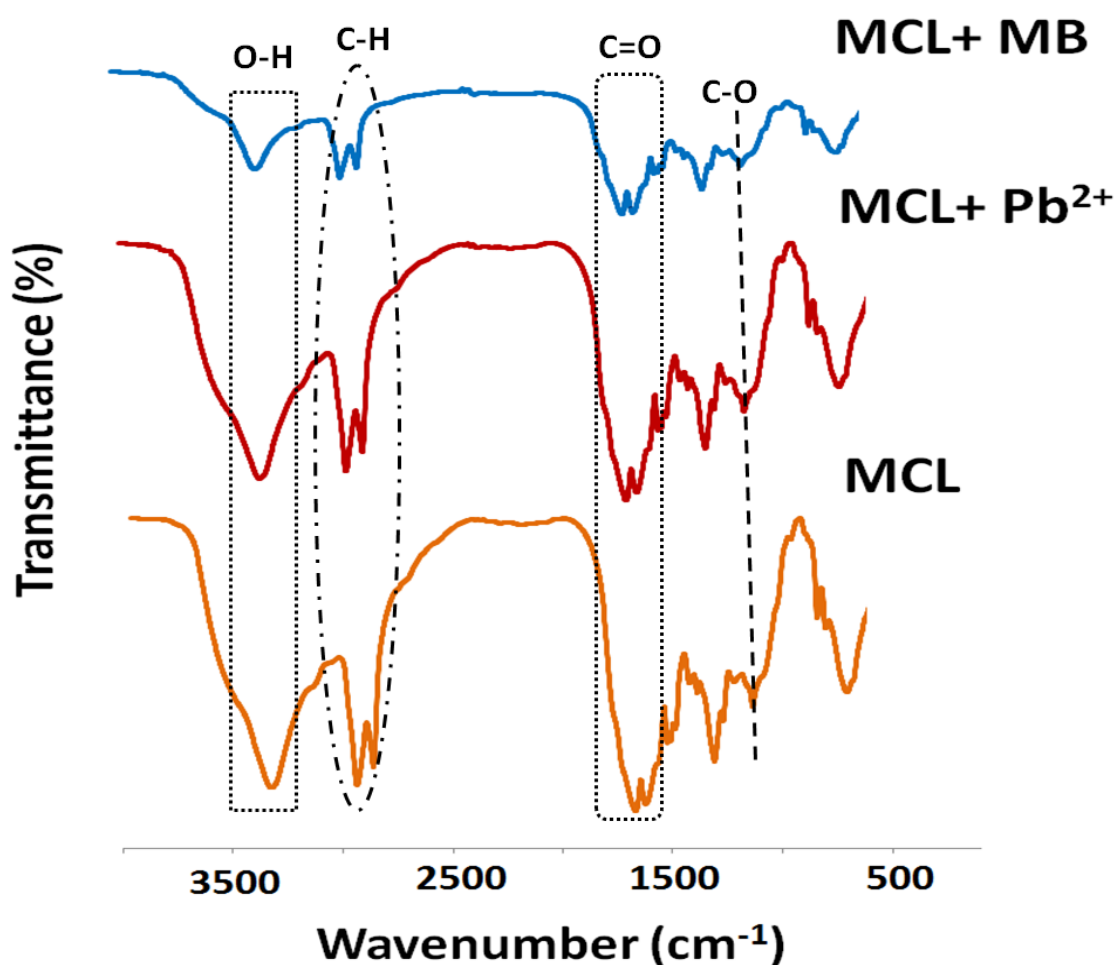


Figure 5.2.2: FTIR spectra for MCL, MCL+MB and MCL+ Pb^{2+}

5.2.3.1.2. SEM-EDX Analysis

The elemental composition and surface morphology of MCL and pollutant loaded MCL were explored with the help of Scanning Electron Microscope coupled with Energy Dispersive Spectrometer, as shown in **Figure 5.2.3**. SEM analysis of MCL indicates a slightly smoother surface with active sites contributing to large surface area facilitating the process of pollutants adsorption³². The morphology of MB and Pb²⁺ loaded bioadsorbent has been represented in **Figure 5.2.3 (I)**. According to EDS analysis of MCL the carbon and oxygen dominate the composition and presence of nitrogen confirms the urethane linkage with *Citrus limetta* surface (**Figure 5.2.3 (II)** and **Table 5.2.1**). The presence of elements complementary with adsorbate molecules appears in EDS spectra represents transfer of dye molecules from solution to bioadsorbent. Relatively higher content of carbon over other elements represents good adsorption capacity of MCL.

Table 5.2.1: Elemental composition of MCL bioadsorbent before and after adsorption of MB and Pb²⁺

Material	C (wt-%)	N (wt-%)	O (wt-%)	Mg (wt-%)	Ca (wt-%)	S (wt-%)	Pb (wt-%)	Cl (wt-%)
MCL	70.84	2.31	26.69	0	0	0	0	0.16
MCL+MB	63.32	3.46	31.87	0.17	0.64	0.11	0	0.21
MCL+Pb ²⁺	60.08	2.28	31.41	0.11	0.73	0	5.39	0

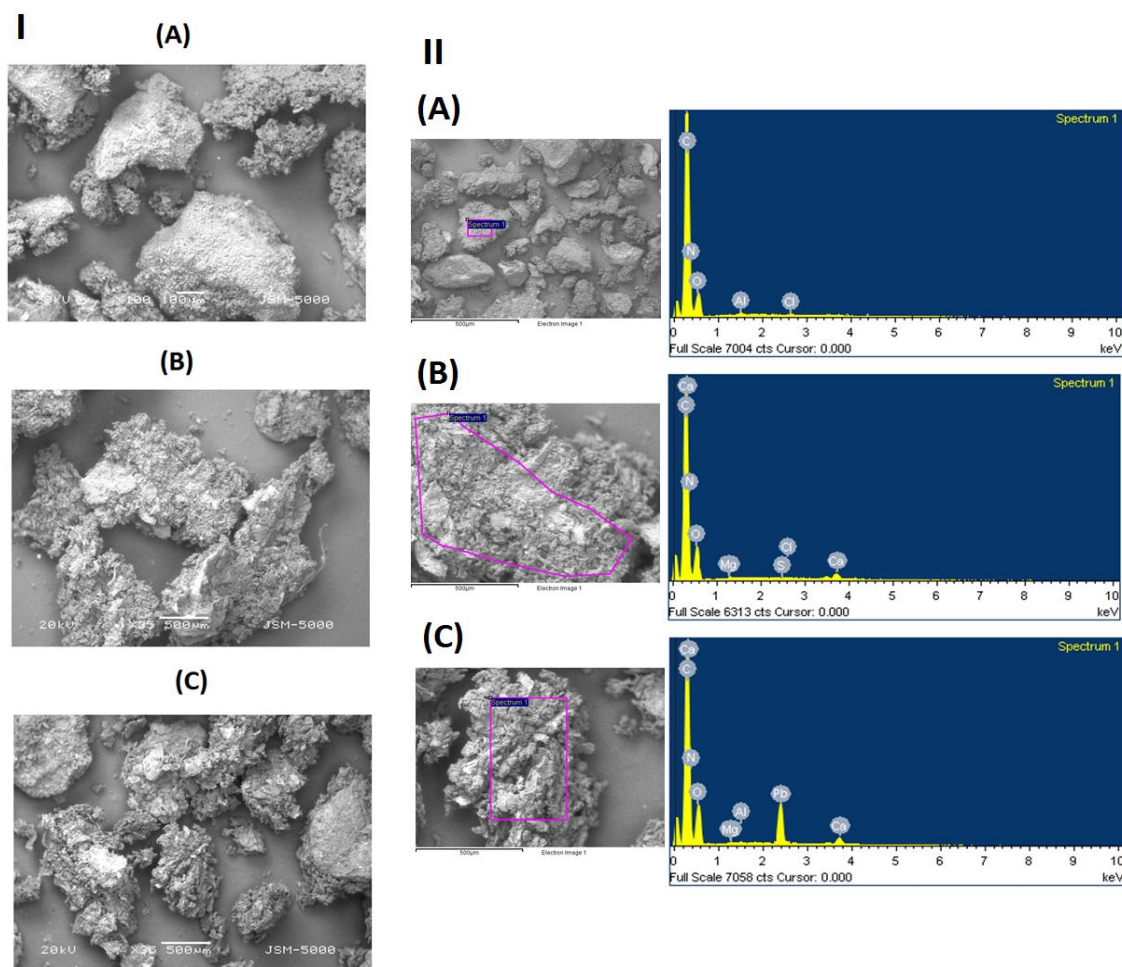


Figure 5.2.3: (I) SEM images of (A) MCL, (B)MCL+MB and (C) MCL+Pb²⁺; (II) EDS curves of (A) MCL, (B) MCL+MB and (C) MCL+Pb²⁺

5.2.3.1.3. BET Analysis

The nitrogen adsorption-desorption isotherm at -196°C result of MCL bioadsorbent has been shown in **Figure 5.2.4**. According to the results obtained, the form of isotherm represents type II plots as per the IUPAC classification. The specific surface area and pore volume of MCL bioadsorbent was found as 2.98 m²/g and 0.00354 cm³/g. The adsorption average pore size distribution was found as 10.53 nm³³. The pores fall in the range of mesoporous structure showing possibility of monolayer adsorption³⁴.

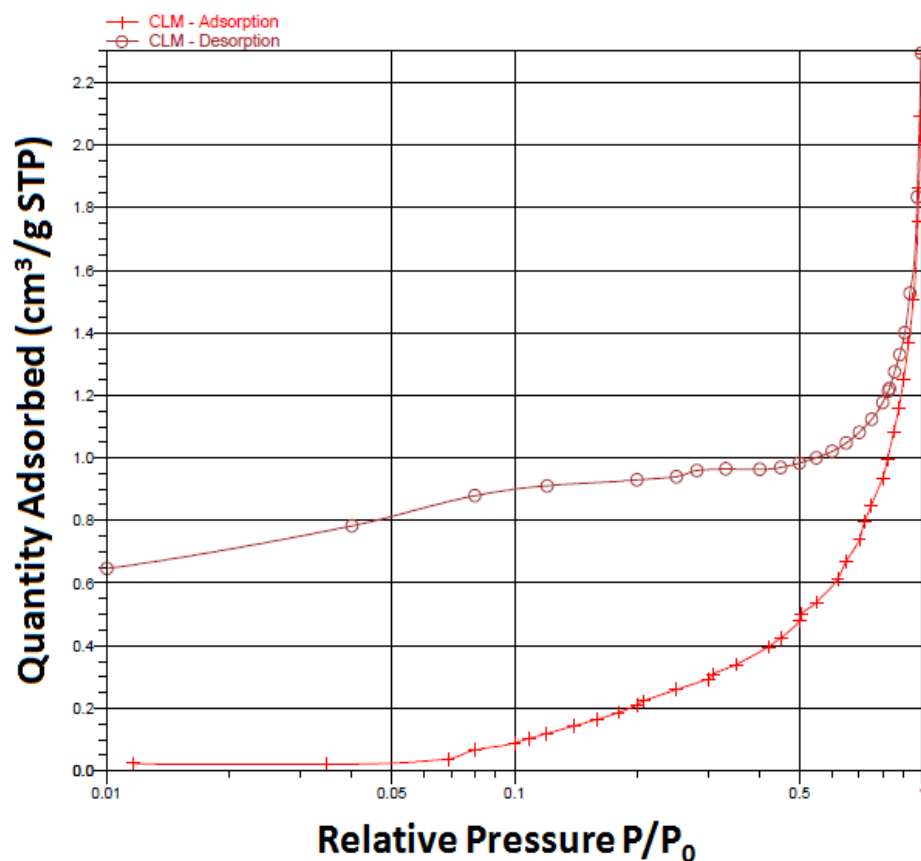


Figure 5.2.4: Nitrogen adsorption-desorption isotherm of MCL bioadsorbent

5.2.3.1.4. TGA Analysis

The thermal decomposition of MCL bioadsorbent was explored in the range of 30-550°C that represents three stages of mass loss as shown in **Figure 5.2.5**. The first stage mass loss of 12.7% was attributed with the presence of moisture content in the temperature range of 30-110 °C. Second stage degradation was detected in the range of 110-360 °C showing major mass loss i.e. 56.6% associated with the decomposition of biomass compounds such as cellulose, hemicelluloses and breakdown of urethane linkage³⁵. The last stage mass loss of 14.9% after 360 °C shows the degradation of organic matter associated with bioadsorbent with higher thermal stability.

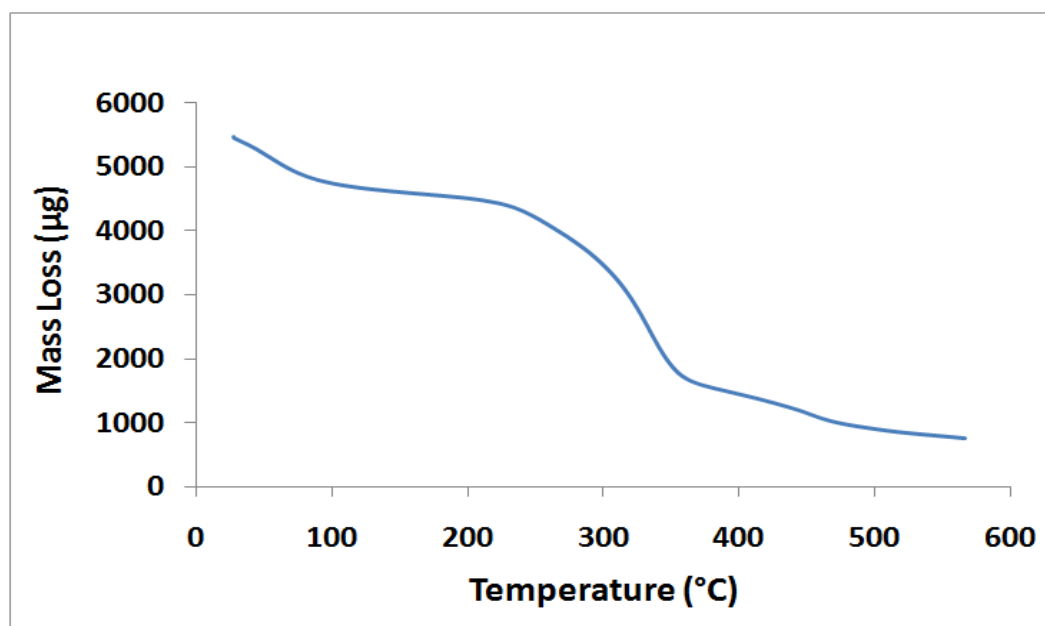


Figure 5.2.5: Thermogravimetric curves for MCL bioadsorbent

5.2.3.1.5. DLS Analysis

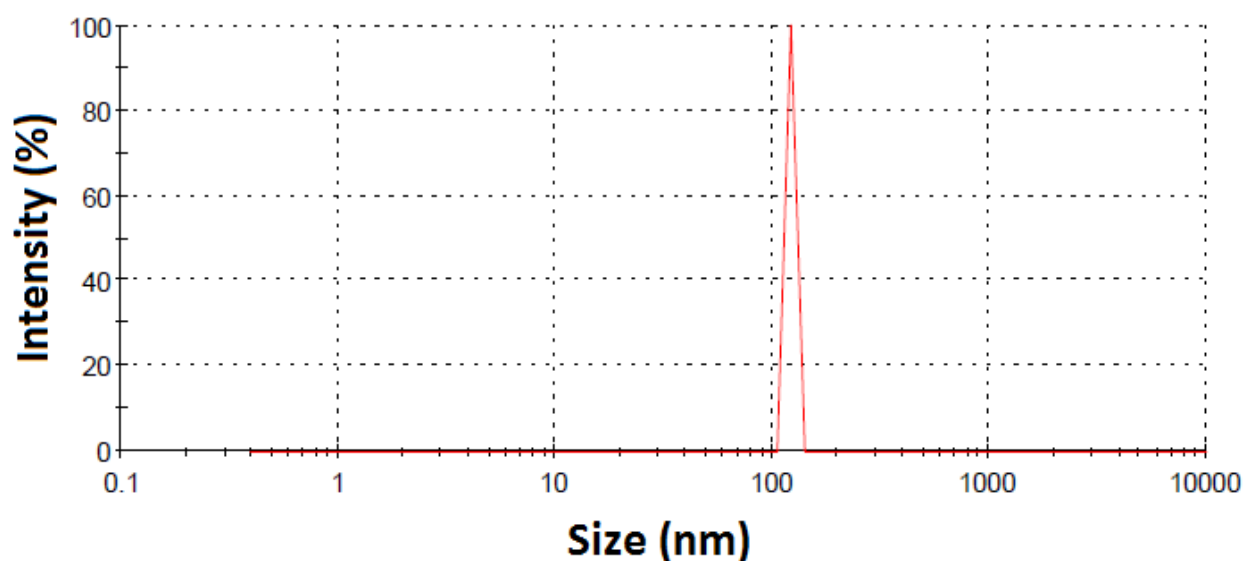


Figure 5.2.6: DLS size distribution diagram of MCL bioadsorbent

The particle size of MCL bioadsorbent was investigated by using Dynamic Light Scattering (DLS) measurement. The hydrodynamic diameter of MCL bioadsorbent recorded at 25 °C was found as 122.4 nm as shown in **Figure 5.2.6**.

5.2.3.1.6. XRD Analysis

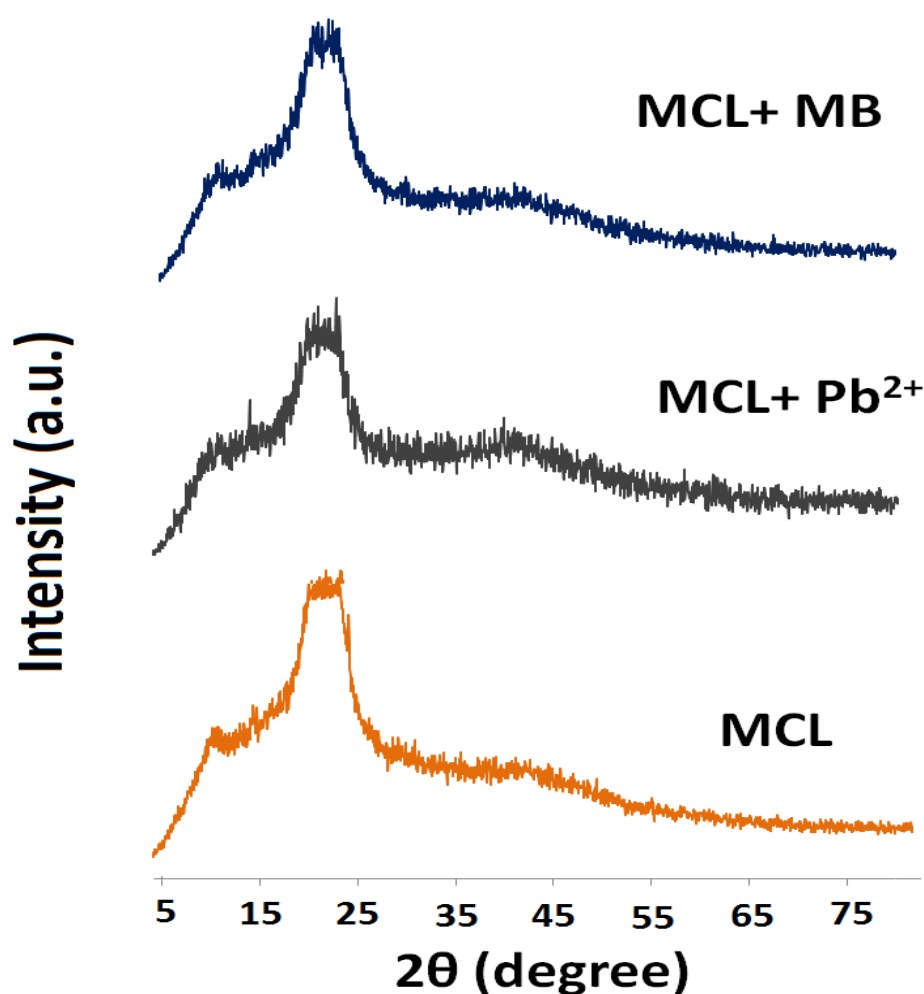


Figure 5.2.7: XRD spectra of MCL, MCL+Pb²⁺ and MCL+MB

The X-ray diffraction pattern of MCL, MCL+Pb²⁺ and MCL+MB has been represented in **Figure 5.2.7**. Between (2θ) 15 to 25°, the broad peaks are associated with highly organized crystalline cellulose content of bioadsorbent. The amorphous nature of bioadsorbent has been shown by weak peaks³⁶. Less organized polysaccharide structure was represented with very small peaks around 16°³⁷. According to the XRD pattern, no change was observed in crystal structure of the particles after adsorption of MB and Pb²⁺. The original peaks of MCL were maintained even after adsorption ensuring the structural stability of bioadsorbent³⁸. This was also confirmed by the FTIR data of pollutant loaded MCL.

5.2.3.2. Effect of MCL Dosage

The quantity of adsorbent plays crucial role in process of adsorption as it corresponds to the available active sites. The availability of several active sites and functional groups can be utilized at higher dosage of adsorbent ultimately increasing the adsorption capacity. The results of this study have been shown in **Figure 5.2.8**. It has been investigated that removal efficiency increases from 62.63% to 98.96% and 57.4% to 91.2% in case of MB and Pb^{2+} , respectively with increasing bioadsorbent quantity from 25 mg to 200 mg. The ideal bioadsorbent dosage for both MB and Pb^{2+} were selected as 100mg for 100 mg/L of their respective solutions.

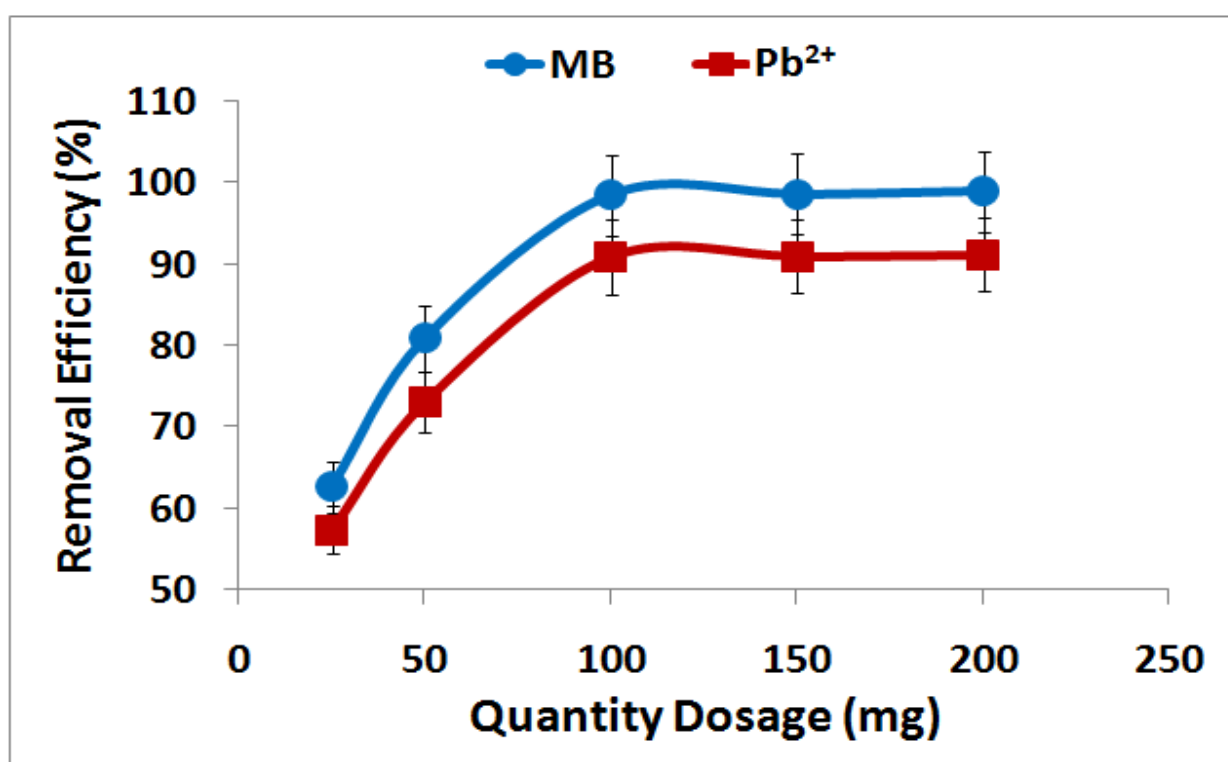


Figure 5.2.8: Effect of MCL dosage on the percentage removal of 100 mg/L of MB and Pb^{2+} at 35°C

5.2.3.3. Effect of Initial Concentration

The impact of initial concentration on equilibrium adsorption capacity and removal efficiency was investigated in the range of 50-250 mg/L (**Figure 5.2.9**). It was observed that removal efficiency increases rapidly before optimum concentration i.e. 100 mg/L for MB and Pb^{2+} then

decreases with increasing initial concentration. In case of MB the reduction of removal efficiency is from 97.8% to 74.27% and for Pb^{2+} the decrement is from 88% to 60.8%. The adsorption capacity rises from 48.9 to 202.92 mg/g for MB and 44 to 152 mg/g for Pb^{2+} with rising initial concentration from 50 to 250 mg/L. The rapid organic and inorganic pollutant adsorption is due to enhanced mass gradient among adsorbate and adsorbent because of increasing concentration. The transport of pollutant molecules from bulk of the solution to the surface of bioadsorbent is induced by mass transfer gradient. After attainment of equilibrium, the decrease in removal efficiency with increasing concentration is due to repulsive force between pollutant molecules on bioadsorbent surface and those in bulk solution. The reduction in number of free active sites for adsorption and incapability of saturated sites to capture pollutant molecules does not favor further adsorption describing the decreasing nature of the graph.^{39,40}

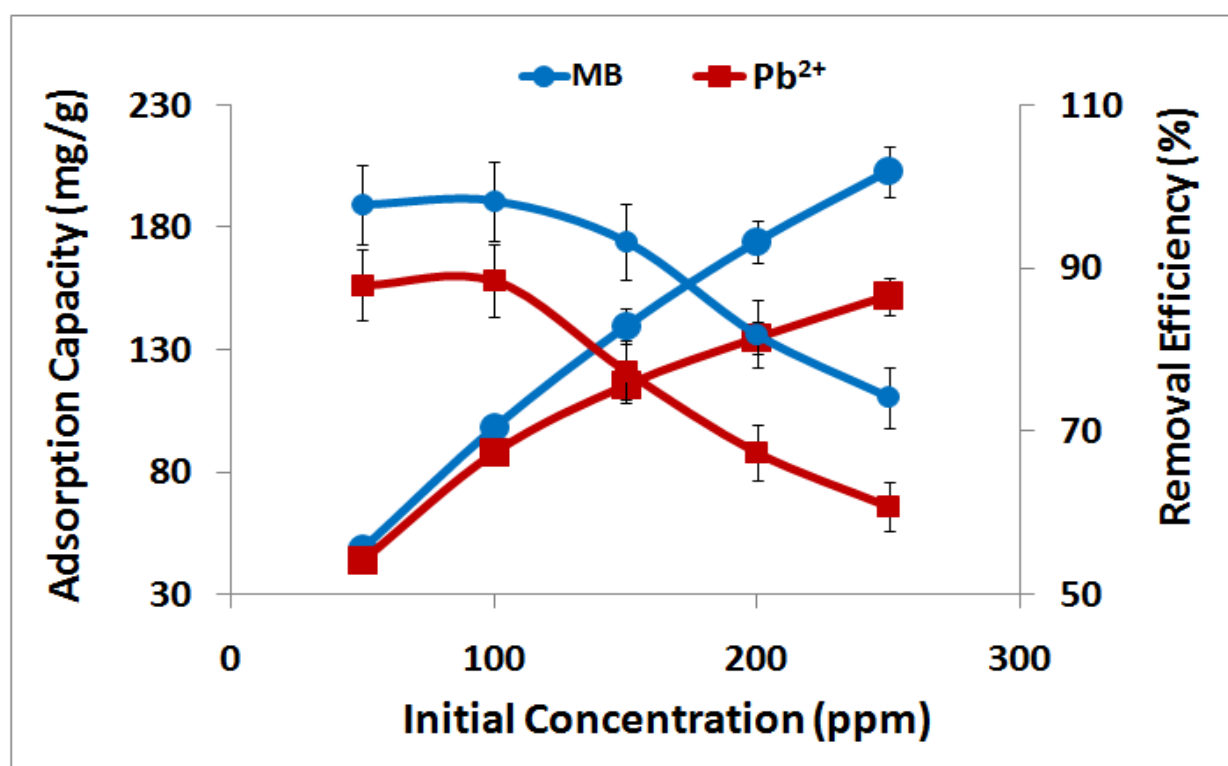


Figure 5.2.9: Effect of initial concentration of MB and Pb^{2+} on adsorption capacity and removal efficiency using MCL at 35°C

5.2.3.4. Effect of pH

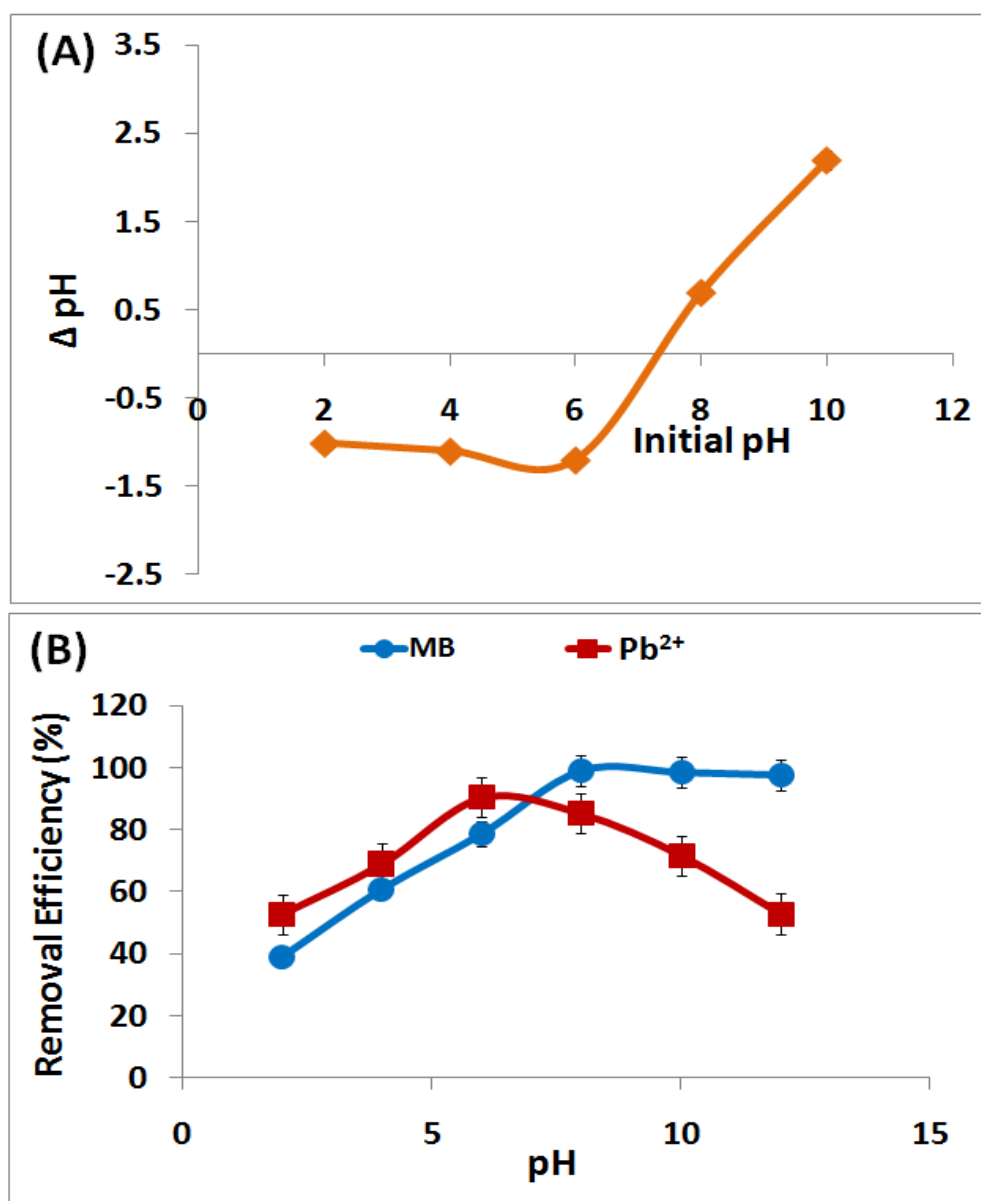


Figure 5.2.10: (A) point zero charge (pH_{PZC}) estimation, (B) Effect of pH on removal efficiency of MB and Pb^{2+} on MCL at 35°C

Initial pH is a significant parameter of adsorption process for removal of organic and inorganic pollutants which directly influences the adsorption capacity. The variation in solution pH may result in change of ionization degree of adsorbate, surface charges associated with adsorbent and level of functional group dissociation on bioadsorbent active sites⁴¹. Point of zero charge (pH_{PZC}) has been investigated to determine the charge associated with bioadsorbent. The estimation of

pH_{PZC} and effect of pH variation on removal efficiency has been represented in **Figure 5.2.10** and explained due to pH_{PZC} . The cationic dye, MB shows higher removal efficiency in higher pH (basic condition) due to negatively charged functional group on bioadsorbent surface. In case of Pb^{2+} , the removal efficiency increases with increasing pH upto neutral condition and decreases in alkaline condition. The removal efficiency of MB increases from 38.8% to 97.5% with rising pH and shows maximum removal efficiency at pH 8 i.e. 98.9%. For Pb^{2+} , the removal efficiency increases from 52.8% (pH 2) to 90.4% at pH 6 and decreases again with increasing pH.

The pH_{PZC} is a facile index to investigate whether the surface charges of bioadsorbent are positive or negative. The pH_{PZC} of the bioadsorbent (MCL) was found to be 7.2, indicating that bioadsorbent will acquire positive charge on their surface on $pH < 7.2$, net zero charge at $pH = 7.2$ and negative charge at $pH > 7.2$. Cationic model adsorption will be favored at $pH > pH_{PZC}$ whereas anionic model adsorption will be favored at $pH < pH_{PZC}$ ²⁵. The adsorption of positively charged MB has been strongly favored at pH more than pH_{PZC} i.e. on negatively charged bioadsorbent surface. The optimum pH for MB adsorption has been fixed to pH 8 as no significant variation in removal efficiency has been observed with increasing pH. The removal efficiency of Pb^{2+} at low pH is less due to competition of H^+ ions with exchangeable cations on MCL surface. With increasing pH, the weak competitive adsorption of H^+ ions in comparison to Pb^{2+} increases the rate of adsorption. Generally aqueous solution of heavy metals exist in form of hydroxides in neutral to alkaline conditions leading to precipitation in the form of $Pb(OH)_2$. Therefore, the removal efficiency of Pb^{2+} varies with increasing pH and pH 6 is considered as optimum pH for Pb^{2+} adsorption⁴².

5.2.3.5. Effect of Contact Time

Figure 5.2.11 shows the impact of contact time on the process of adsorption of pollutants i.e. MB and Pb^{2+} by MCL at 1, 2, 3, 5 and 7 hours (pH 8 for MB and pH 6 Pb^{2+}). Removal efficiency of MB and Pb^{2+} at the end of 7 hours was investigated as 95.13% and 89.5%, respectively. In general, the carboxyl group can effectively adsorb the heavy metal ions. The removal efficiency increases rapidly in initial stage due to abundance of unoccupied active functional sites on bioadsorbent and adsorbate molecules migrate from solution to adsorbent surface. The adsorption process could be explained by electrostatic interaction and hydrogen bonding in between cationic pollutants and adsorbent. The adsorption process begins with increasing

removal efficiency with time via Van der Waals forces and closer proximity of bioadsorbent with cationic pollutant molecules lead to electrostatic interactions. Near equilibrium, between 5 to 7 hours the removal efficiency becomes sluggish due to saturation of active sites. The decreased and constant removal rate occurs due to the inability of cationic pollutant molecules to occupy the free active sites of the bioadsorbent surface because of repulsive forces of adsorbate molecules between the bulk of solution and solid phase. Slower diffusion rate of adsorbate molecules onto adsorbent and electrostatic hindrance also contribute to slower rate of removal near equilibrium. Similar finding has been reported for adsorption with respect to time⁴³.

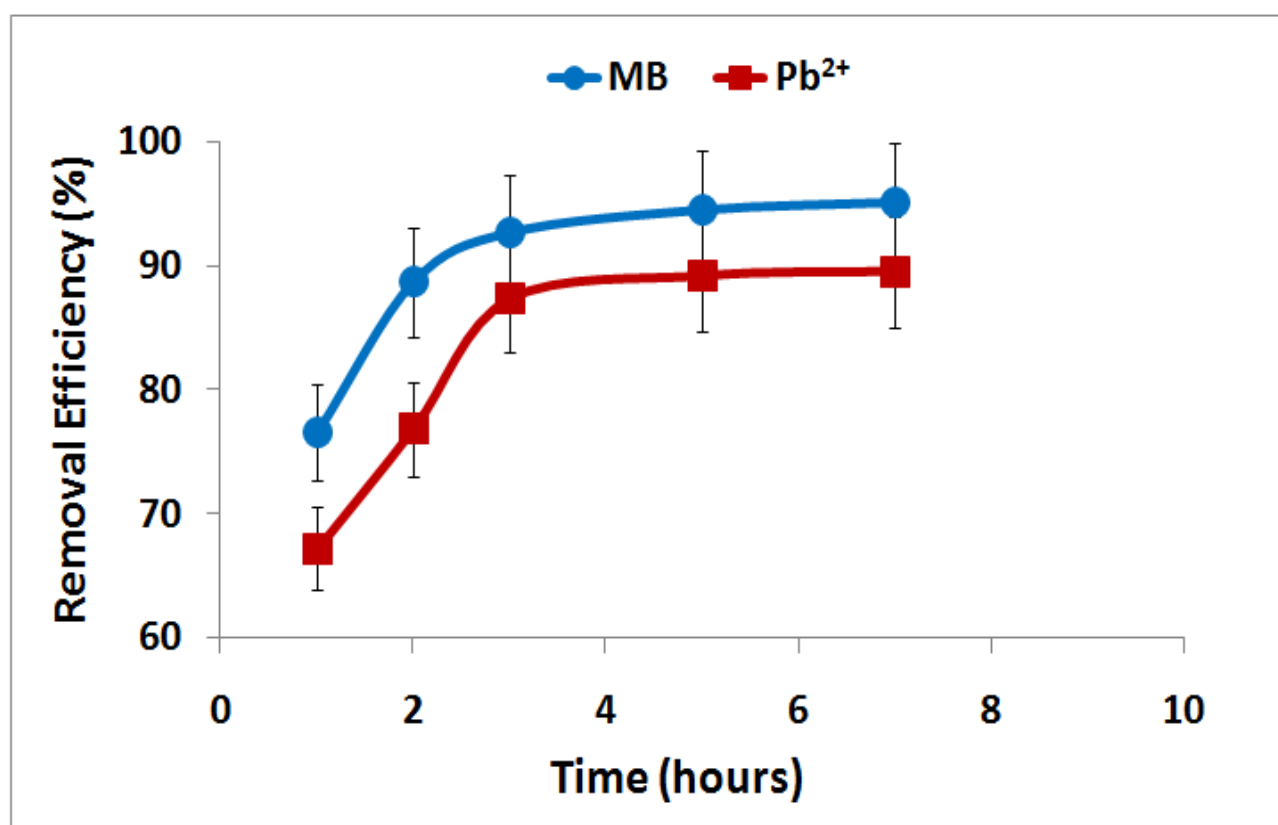


Figure 5.2.11: Effect of contact time on the percentage removal of 100mgL⁻¹ of MB and Pb²⁺ at pH-6.0 and pH- 8.0, respectively at 35°C

5.2.3.6. Effect of Temperature

The temperature variation has an effective role in increasing or decreasing the adsorption process. In this system, removal efficiency increases with increasing temperature as represented

in **Figure 5.2.12**. In case of MB the removal efficiency increases from 97.24% to 99.02% and 86.9% to 91.9% for Pb^{2+} with rise in temperature from 35°C to 55°C. The investigated result suggested that adsorption of MB and Pb^{2+} on MCL is an endothermic process as adsorption is favored at higher temperature. The increase of adsorption with increasing temperature might be associated with increase in mobility of adsorbate molecules with temperature and also provide sufficient energy for interaction of adsorption site of bioadsorbent surface and adsorbate molecules³⁴. A similar trend was also observed in some reported works of adsorption^{6,27}.

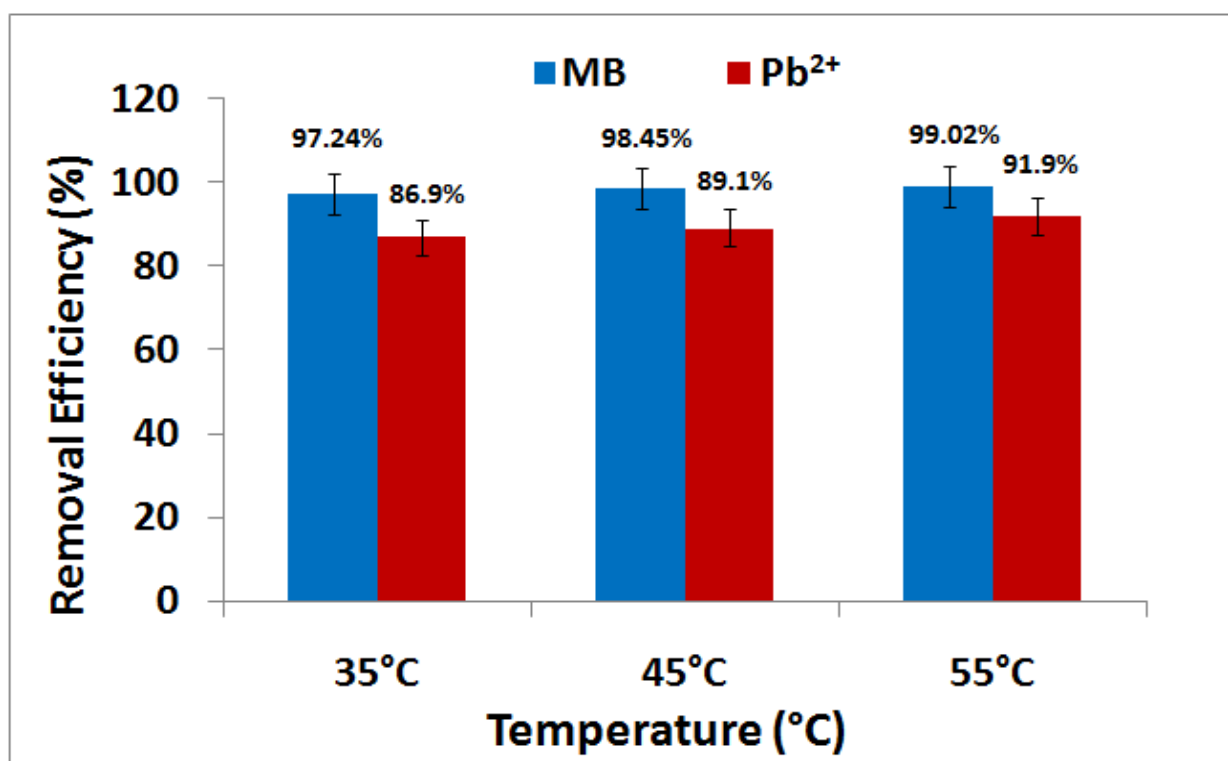


Figure 5.2.12: Effect of temperature on dye removal efficiency with increasing temperature from 35 °C to 55 °C

5.2.3.7. Adsorption Isotherms

Adsorption isotherm is considered as one of the crucial parameters of adsorption process. Generally, the adsorption isotherm on the basis of adsorption equilibrium was used to estimate performance of adsorbent. The relationship between adsorbate equilibrium concentration (C_e) and per unit gram of adsorption capacity at equilibrium (Q_e) at constant temperature represents adsorption isotherm⁴⁴. They are imperative for designing an adsorption system, its data analysis and shows extensive interpretation of the nature of interaction. In this context, adsorption

capacities of MB and Pb^{2+} onto MCL were investigated using Langmuir and Freundlich adsorption isotherm models (Figure 5.2.13).

$$\frac{C_e}{q_e} = \frac{1}{K_L} + \frac{C_e}{q_m} \dots \dots \dots (5)$$

$$\log q_e = \log K_F + \frac{1}{n} \log C_e \dots \dots \dots (6)$$

where, C_e (mg L^{-1}) and q_e (mg g^{-1}) is the equilibrium concentration of dyes and adsorption capacity of MCL at equilibrium, respectively; q_m is the maximum adsorption capacity (mg g^{-1}), $1/n$ represents constant associated with adsorption intensity variation with heterogeneity of adsorbent and K_L (L/mg) and K_F (L/mg) are the Langmuir and Freundlich equilibrium adsorption constants, respectively. The value of K_L represents whether the adsorption is favorable, unfavorable or linear under the condition of ($0 < K_L < 1$), ($K_L > 1$) and ($K_L = 1$), respectively²⁸.

The calculated data of Langmuir and Freundlich isotherm model has been represented in Table 5.2.2. The experimental data fitted well into both adsorption isotherm model i.e. Langmuir and Freundlich model. On the basis of correlation co-efficient, Langmuir adsorption isotherm model fitted better than Freundlich model representing monolayer adsorption process for both adsorbates. In monolayer adsorption process, certain homogeneous sites on the adsorbent facilitates adsorption and all these sites are energetically identical⁴⁵.

Table 5.2.2: Isotherm constants for the adsorption of 100mgL^{-1} of MB and Pb^{2+} at 35°C

Dye Molecule	Langmuir				Freundlich		
	Q_m (mg g^{-1})	K_L (L mg^{-1})	R^2	R_L	$1/n$	K_F (L mg^{-1})	R^2
MB	250	0.2352	0.992	0.0407	0.321	62.37	0.873
Pb^{2+}	200	0.0568	0.993	0.1496	0.369	29.99	0.817

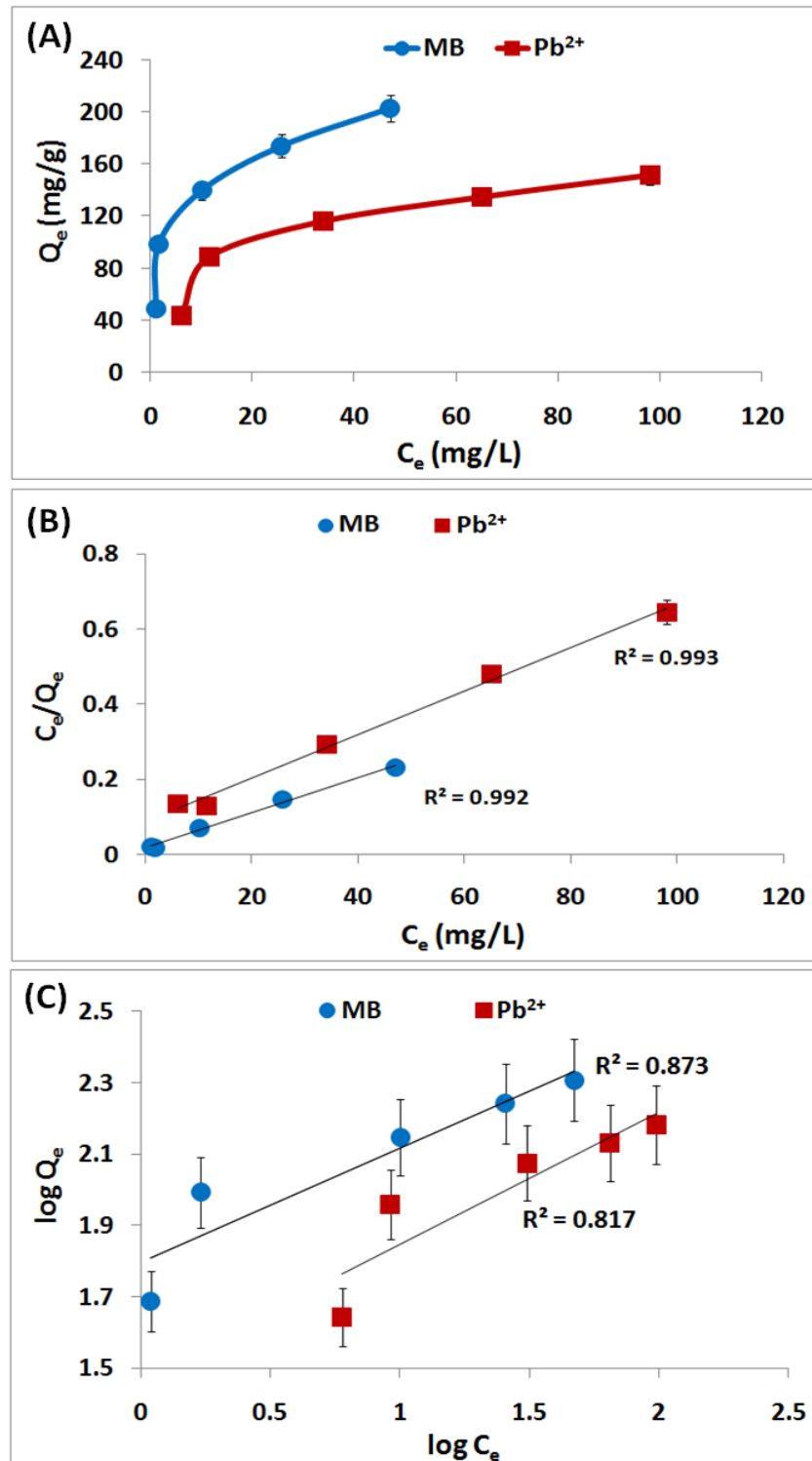


Figure 5.2.13: (A&B) Langmuir and (C) Freundlich adsorption isotherm for the removal of 100mgL^{-1} of MB and Pb^{2+} at 35°C

5.2.3.8. Adsorption Kinetics

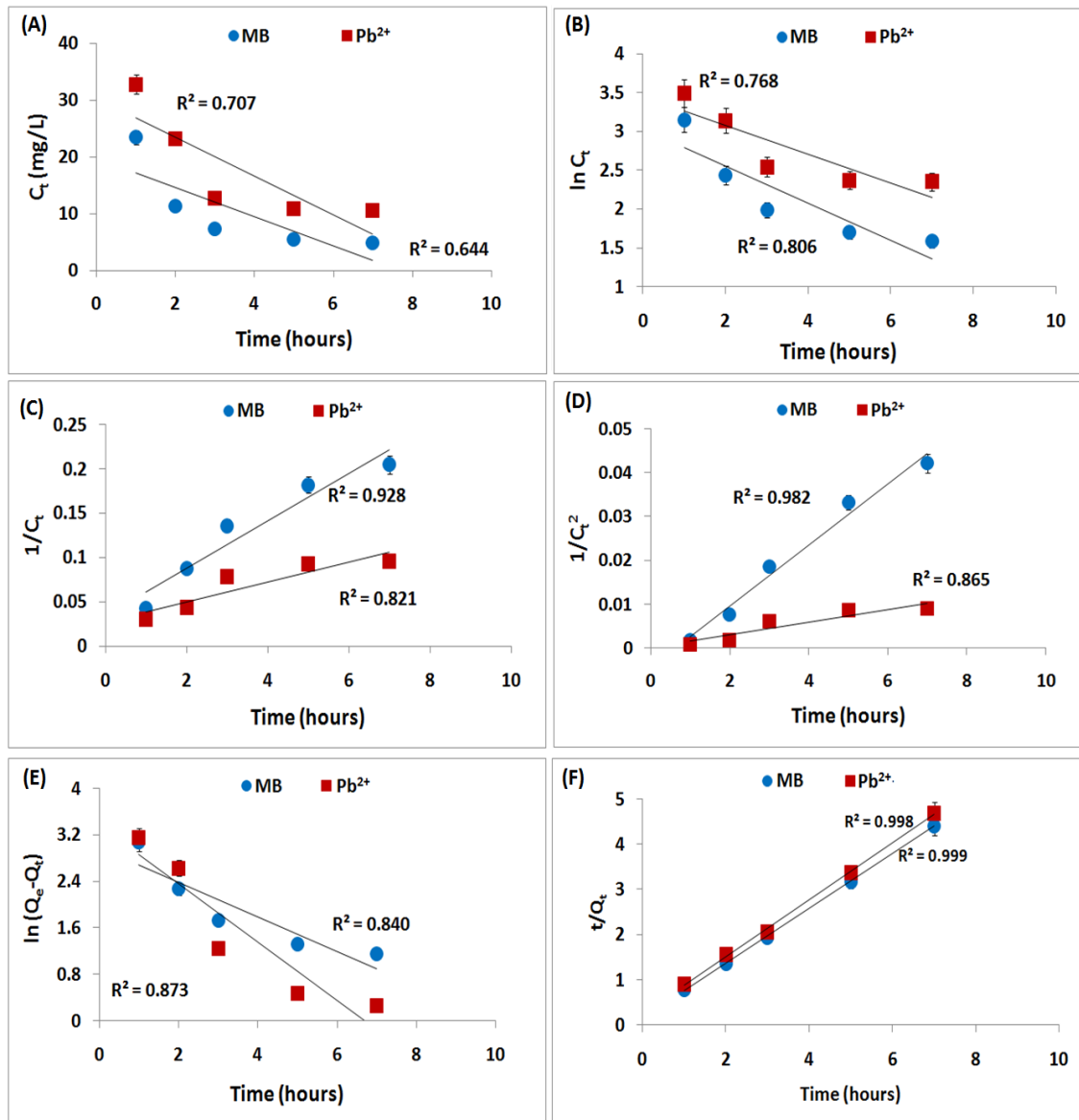


Figure 5.2.14: Graphs of (A) Zero order (B) First Order (C) Second Order (D) Third Order (E) Pseudo first order (F) Pseudo Second Order kinetic curves for MB and Pb²⁺ adsorption on MCL

Adsorption kinetics is very crucial study for practical applications, control of operation and designing process since it provides significant insights into pathway of reaction as well as mechanism of adsorption process. Solute uptake has been described by kinetics by controlling the time of adsorbate uptake at interface of solid and solution. Several kinetic models have been

implemented on experimental data, such as Zero order, First order, second-order, third order, pseudo-first order, pseudo second order models. On the basis of correlation co-efficient it was concluded that data fitted well with the pseudo- second order model as shown in **Figure 5.2.14**.

$$\ln(q_e - q_t) = \ln q_e - k_1 t \dots \dots \dots (7)$$

$$\frac{t}{q_t} = \frac{1}{k_2 q_e^2} + \frac{t}{q_e} \dots \dots \dots (8)$$

Here, q_e is the adsorbed dye amount at equilibrium, q_t (mg g^{-1}) is the adsorbed dye amount at time t (minutes). k_1 and k_2 (mg min g^{-1}) are the rate constant of pseudo-first order and pseudo-second order kinetic models. The experimental data follow the pseudo second order model with correlation coefficient of 0.999 for MB and 0.998 for Pb^{2+} . **Table 5.2.3** represents the kinetic parameters of MB and Pb^{2+} adsorption. This suggested that the adsorption of organic and inorganic pollutant is influenced by its chemical interactions with bioadsorbent revealing that chemisorption is the rate determining step ⁴⁶.

Table 5.2.3: Kinetics parameters for adsorption of MB and Pb^{2+} on MCL

Pollutants	Pseudo First Order			Pseudo Second Order		
	Q_e (mg/g)	k_1 (10^{-5})	R^2	Q_e (mg/g)	k_2 (10^{-3})	R^2
MB	19.68	-1.19	0.84	100	0.68	0.999
Pb^{2+}	28.76	-1.90	0.873	100	0.4	0.998

5.2.3.9. Adsorption Thermodynamics

The adsorption thermodynamics is an important parameter to evaluate whether the adsorption process is spontaneous or not. It is also utilized to investigate the mechanism of adsorption. The data obtained from adsorption experiments at different temperatures i.e. 35°C , 45°C and 55°C were estimated using thermodynamics equations. Several parameters like Gibbs free energy (ΔG°), change in entropy (ΔS°) and enthalpy change (ΔH°), were calculated from thermodynamic equilibrium constant (K_c) using appropriate equations as mentioned below:

$$K_c = \frac{a_s}{a_e} = \frac{\vartheta_s q_e}{\vartheta_e C_e} \dots \dots \dots (9)$$

where, a_s denotes activity of the adsorbate molecules adsorbed on the surface of bioadsorbent and a_e represents its activity within solution at equilibrium; v_s is activity coefficient of adsorbate adsorbed in solution and v_e represents the activity coefficient of the adsorbate molecules at equilibrium.

The activity coefficient v reaches closer to unity when concentration of adsorbate solution decreases and approaches zero, under this situation the above equation could be represented as:

$$\lim_{c_e \rightarrow 0} \frac{a_s}{a_e} = \frac{q_e}{c_e} = K_c \dots\dots\dots (10)$$

The values of ΔH° and ΔS° have been calculated from intercept and slope of Van't Hoff plot of experimental data $\ln K_c$ versus $1/T$ at three different temperatures i.e. 308, 318 and 328 K. The thermodynamic surface plot and Van't Hoff plot has been shown in **Figure 5.2.15**. Then Gibbs free energy has been calculated as per the equation 11.

$$\Delta G^\circ = -RT \ln(K_c) \dots\dots\dots (11)$$

$$\ln K_c = \frac{\Delta S^\circ}{R} - \frac{\Delta H^\circ}{R} \cdot \frac{1}{T} \dots\dots\dots (12)$$

The negative values of ΔG° at different temperatures reveal the spontaneous nature of MB and Pb^{2+} adsorption on MCL. More negative values with increasing temperature represent more energetically favored process of adsorption. The studies exhibit an increase in negative value of ΔG° with increasing temperature as shown in **Table 5.2.4**. The positive ΔS° value shows enhanced randomness during the process of adsorption at solid-solution interface. The positive value of ΔH° suggested endothermic nature of the adsorption process associated with bioadsorbent. It is also reported that physisorption process has been represented by 2.1–20.9 kJ mol⁻¹ value of ΔH° and values lying between 80-200 kJ mol⁻¹ for chemisorption process. Since the calculated values are more than 20.9, the process of organic and inorganic pollutant removal via bioadsorbent follows chemisorption. This corroborates with the kinetics modelling obtained.

47

Table 5.2.4: Thermodynamic parameters for the adsorption of MB and Pb^{2+} on MCL

Contaminants	K_c			ΔH°	ΔS°	ΔG°		
	308 K	318 K	328 K			308 K	318 K	328 K
MB	35.26	63.53	101.15	44.29	0.173	-9.12	-10.97	-12.58
Pb^{2+}	6.63	8	11.34	22.19	0.087	-4.83	-5.552	-6.599

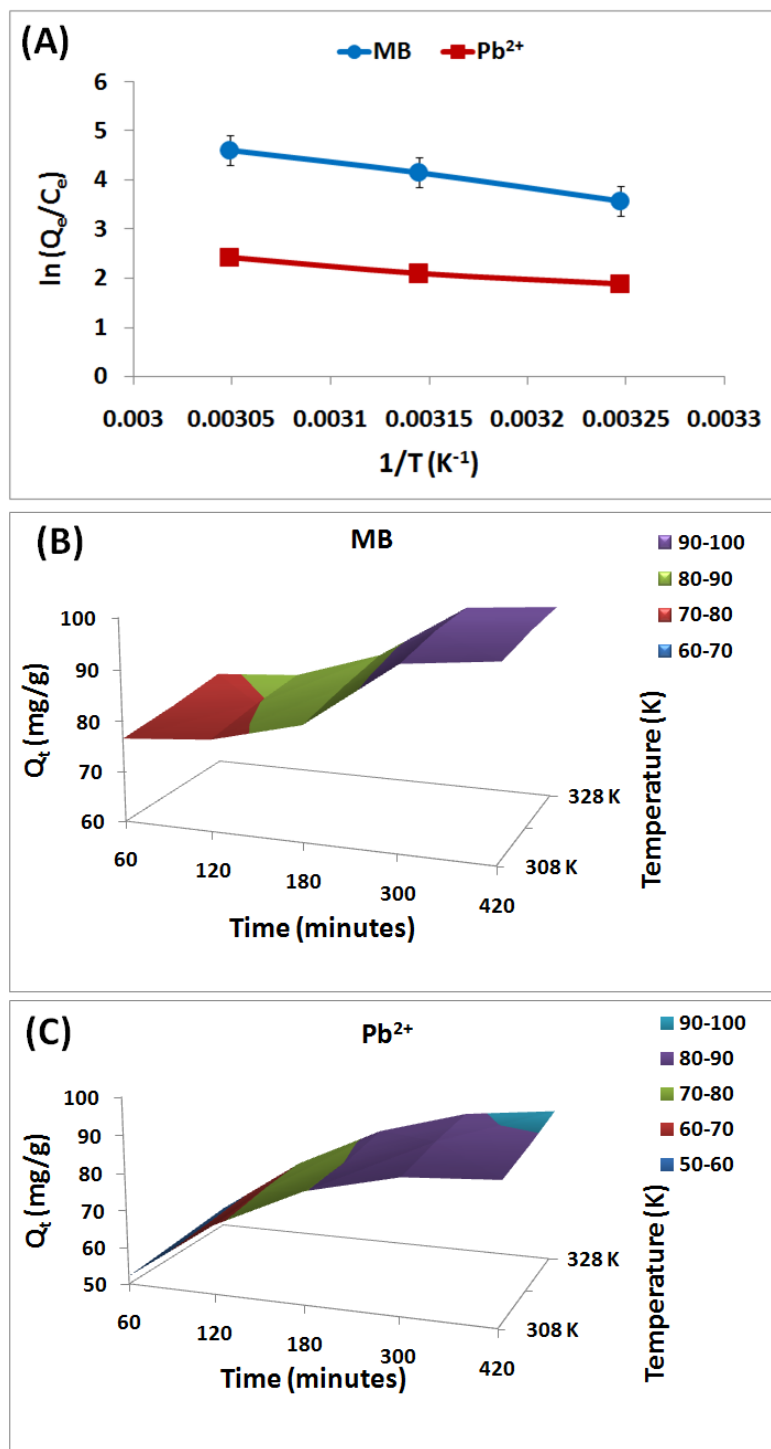


Figure 5.2.15: (A) $\ln(Q_e/C_e)$ versus $1/T$ graph for estimation of thermodynamic parameters for adsorption of MB and Pb^{2+} , (B&C) Thermodynamic surface plots of MB and Pb^{2+} , respectively

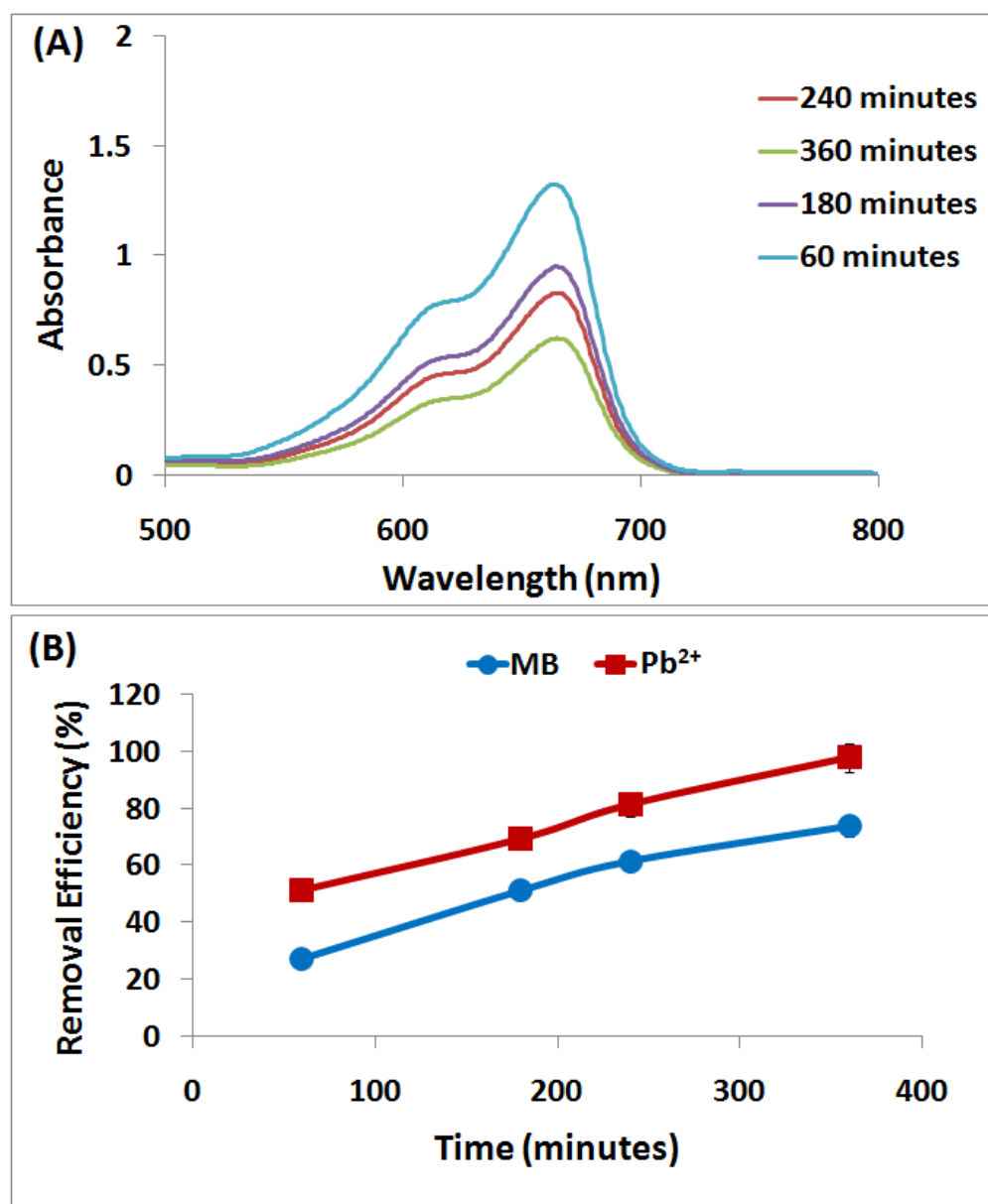
5.2.3.10. Simultaneous Adsorption Study of MB and Pb^{2+} 

Figure 5.2.16: (A) UV-vis spectra of MB in binary solution with time and (B) Removal Efficiency of MB and Pb^{2+} with time in binary solution

The results of simultaneous adsorption of MB and Pb^{2+} represents that Pb^{2+} has higher adsorption capacity in comparison to MB in binary solution. The removal efficiency of MB and Pb^{2+} was investigated as 73.93% and 97.86% respectively, as shown in **Figure 5.2.16**. The simultaneous adsorption effect of organic and inorganic pollutants on MCL was investigated by utilizing the ratio of adsorption capacities (Rq):

$$R_q = \frac{q_{b,i}}{q_{m,i}} \dots \dots \dots (13)$$

where, $q_{b,i}$ and $q_{m,i}$ represents the adsorption capacity of system 'i' in the binary and mono-component solution, respectively with same initial concentration.

In case of simultaneous adsorption, three probable conditions occur: i) $R_q < 1$ indicates antagonism, where adsorption of one component is suppressed in the presence of other component; ii) $R_q > 1$ represents synergism suggesting that the adsorption of one component is amplified by the existence of other component and iii) $R_q = 1$ shows non-interaction i.e. the adsorption of component 'i' is not afflicted by the presence of co-pollutant.

In this system, the presence of MB enhances the adsorption of Pb^{2+} whereas, the presence Pb^{2+} reduces the adsorption of MB (i.e. $R_{q, MB} = 0.75$ and $R_{q, Pb^{2+}} = 1.11$). The presence of Pb^{2+} on surface of MCL could not provide extra active sorption sites for MB. The co-existence of MB and Pb^{2+} leads to the competitive adsorption to the binding sites of adsorbent that reduces the adsorption of MB. This phenomenon could be described by the fact that electrostatic attraction of Pb^{2+} with MCL is stronger in comparison to MB in binary adsorption mechanism^{48,49}. Thus, maximum uptake of Pb^{2+} occurs in binary solution due to its stronger affinity with MCL surface.

5.2.3.11. Desorption and Regeneration of MCL

Desorption study is one of the important indices to regenerate the adsorbent as well as recover the adsorbate molecules. It also helps in defining the efficiency of the adsorbent. The successful desorption process requires proper eluents system based on the type of adsorbent and adsorbate interaction. To assess the reusability of bioadsorbent, successive adsorption/desorption cycles were carried out using 0.1M HCl, 0.1M NaOH and Ethanol solution as eluents^{50,51} (**Figure 5.2.17 (A)**). The obtained results, suggested that HCl is better eluent system for desorption in comparison to NaOH and Ethanol. The removal efficiency with HCl was found to be 98.6% for MB and 89% for Pb^{2+} . Results show that the removal efficiency decreases slowly after every cycle (**Figure 5.2.17 (B)**). The FTIR analysis of regenerated MCL exhibits no change in characteristic spectra of bioadsorbent as shown in **Figure 5.2.17 (C)**. This suggests that after successful adsorption of MB and Pb^{2+} , MCL retains its structure enhancing the economic viability of the process.

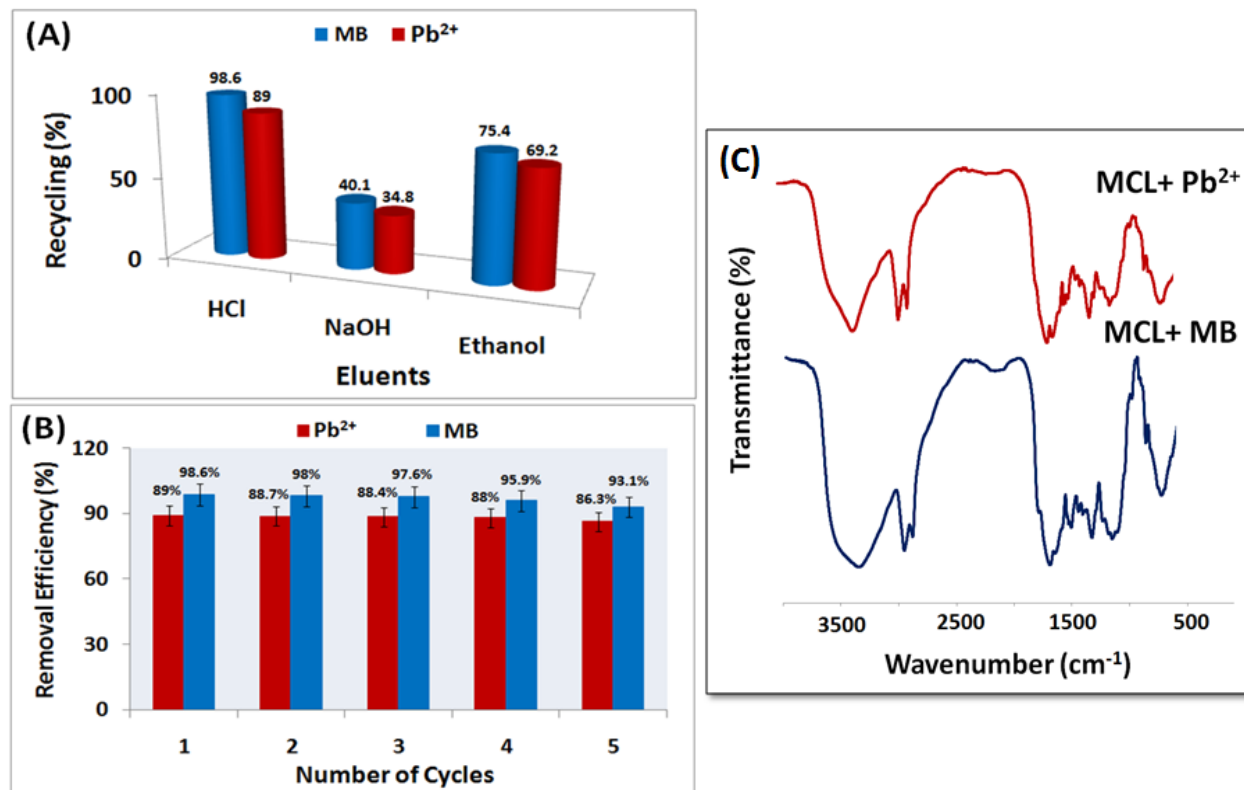


Figure 5.2.17: (A) Desorption study of MB and Pb²⁺ with different eluents; (B) Percentage removal of MB and Pb²⁺ after successive desorption/adsorption cycles using HCl as eluent; (C) FTIR spectra of regenerated MCL after adsorption of MB and Pb²⁺

5.2.3.12. Adsorption Mechanism

The probable interaction of MCL with MB and Pb²⁺ is shown in **Figure 5.2.18**. The adsorption mechanism is governed by several factors such as structural and functional behavior of adsorbate molecules as well as surface characteristics of bioadsorbent including pore volume, surface area, active sites and surface chemical groups⁵². In this system, the adsorbate molecules are cationic pollutants i.e. dye (MB) and heavy metal (Pb²⁺). The bioadsorbent surface has been affirmed by presence of several functional groups such as -COOH, -OH, -NH etc. which in turn govern the process of adsorption. The uptake of Pb²⁺ molecule was regulated by electrostatic interaction and in case of MB, the hydrogen bonding and electrostatic interaction plays major role in adsorption. Since, MB adsorption undergoes both interactions i.e. hydrogen bonding and electrostatic interaction, their adsorption rate is higher than Pb²⁺. The stability of bioadsorbent increases due to strong urethane linkage utilized for cross-linking of native *Citrus limetta* powder. The FTIR

analysis also helps in further investigation of adsorption mechanism. The MCL spectra before and after adsorption of MB and Pb^{2+} were analyzed to detect the functional groups interaction with dye and heavy metal. The slight shift of hydroxyl peak from 3335 cm^{-1} and decrease in its intensity after adsorption confirms the contribution of hydroxyl groups in process of adsorption. The shift of $2\text{--}5\text{ cm}^{-1}$ from 1626 cm^{-1} of --C=O group after adsorption represents the successful removal of pollutants⁵³.

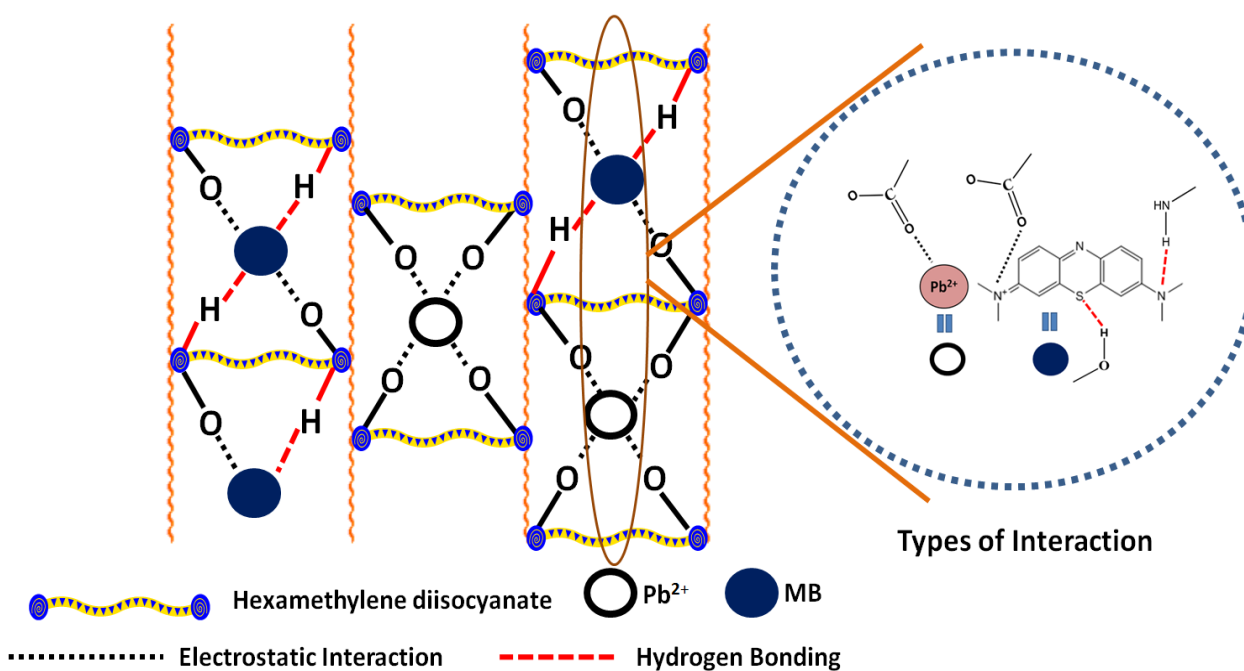


Figure 5.2.18: Probable mechanism of adsorption of MB and Pb^{2+}

5.2.3.13. Adsorption of environmental sample using MCL bioadsorbent

In order to explore the application of MCL bioadsorbent in adsorption of pollutants from real environmental sample, a preliminary study has been conducted. An effluent collected from textile industry has been diluted in the ratio of 1:2 and furthered utilized as adsorbate system. 20 mL of environmental sample was stirred at 160 rpm with 100 mg of MCL bioadsorbent for 7 hours. The resultant UV-visible spectra (**Figure 5.2.19**) represented the decrement in color intensity showing successful removal of color from environmental sample.

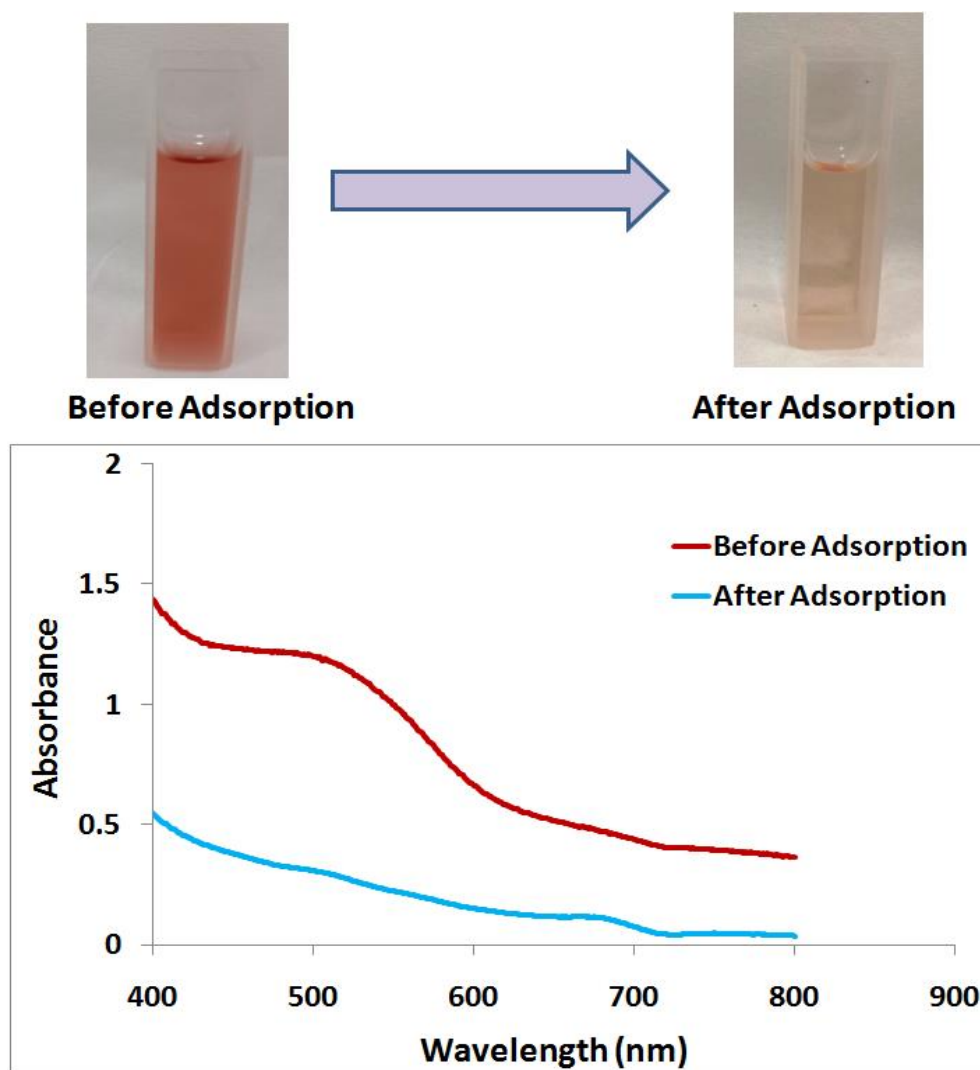


Figure 5.2.19: UV visible spectra of environmental sample adsorption using MCL bioadsorbent

5.2.3.14. Comparison with Other Bioadsorbents

The values of maximum adsorption capacities of the MB and Pb^{2+} on MCL obtained from experimental data have been compared with other reported adsorption capacities in literature (Table 5.2.5). It is observed that MCL has a greater adsorption capability in comparison to other bioadsorbents, suggesting that MCL could be considered as a promising bioadsorbent for removal of organic and inorganic pollutants.

Table 5.2.5: Comparison of maximum adsorption capacities of MCL with other adsorbents

ADSORBENT	ADSORBATE	Qm (mg/g)	Reference
Polyethyleneimine-bacterial cellulose (PEI-BC) bioadsorbent	Cu (II) and Pb (II)	141 mg/g and 148 mg/g	⁵⁴
Saffron flower waste	Pb (II)	45.62 mg/g	⁵⁵
Tomato waste	Pb (II)	152 mg/g	⁵⁶
Wheat straw, Wheat straw biochar, ball-milled wheat straw biochar	Pb (II)	46.33 mg/g, 119.55 mg/g and 134.68 mg/g	²³
<i>Caryocar coriaceum</i> Wittm bark tailings	Pb (II)	106.36 mg/g	⁵⁷
Dragon fruit, Hamimelon and Avocado fruit peels	Alcian Blue, Methylene Blue, Pb ²⁺ and Ni ²⁺	71.85 mg/g, 62.58 mg/g, 7.89 mg/g, 9.45 mg/g	²¹
L-arginine modified magnetic bioadsorbent (Fe ₃ O ₄ -CS-L)	Zn (II), Cd (II) and Pb (II)	256.41 mg/g, 156.99 mg/g and 128.63 mg/g	⁵⁸
Activated carbon/cellulose composite (ACC) biosorbent	MB	103.66 mg/g	⁵⁹
crass seed mucilage (CSM) based magnetic adsorbent	MB	44.6 mg/g	⁶⁰
Banana Peels (BP), Cucumber Peels (CP) and Potato Peels (PP)	MB	211.9 mg/g, 179.9 mg/g and 107.2 mg/g	⁶¹
MCL	MB and Pb (II)	250 mg/g and 200 mg/g	This work

5.2.4. Conclusion

In summary, this work establishes a facile and simple approach to prepare a novel modified *Citrus limetta* (MCL) bioadsorbent that effectively eliminate organic (MB) and inorganic (Pb²⁺) pollutants from aqueous solution as well as removal of color from environmental sample. The results revealed that MCL is an excellent eco-friendly bioadsorbent system for removal of MB and Pb²⁺ with maximum removal efficiency of 99.02% and 91.9% for MB and Pb²⁺,

respectively. The maximum adsorption capacity of MB was found to be 250 mg/g and 200 mg/g for Pb^{2+} . The main advantage of bioadsorbent with urethane linkage was evaluated to enhance its stability and facilitate the adsorption process. The detailed investigation of adsorption using bioadsorbent (MCL) revealed that adsorption process was governed by hydrogen bonding and electrostatic interaction between adsorbate molecules and adsorbent. The detailed investigation of adsorption parameters included concentration, adsorbent dose, pH and temperature variation. The adsorption kinetic studies revealed that adsorption process follows pseudo second order model. The equilibrium experimental data were best fitted with Langmuir isotherm model suggesting monolayer adsorption. The thermodynamic study shows spontaneous and endothermic nature of adsorption process. Furthermore, MCL can be regenerated and reused upto five cycles with slight decrement in removal efficiency. Thus, it can be concluded that Modified *Citrus limetta* could be used as promising bioadsorbent for eliminating organic and inorganic pollutants due to its high efficiency, cost effectiveness and ease of operation.

References

- (1) Kamranifar, M.; Khodadadi, M.; Samiei, V.; Dehdashti, B.; Sepehr, M. N.; Rafati, L.; Nasseh, N. Comparison the Removal of Reactive Red 195 Dye Using Powder and Ash of Barberry Stem as a Low Cost Adsorbent from Aqueous Solutions : Isotherm and Kinetic Study. *J. Mol. Liq.* **2018**, *255*, 572–577. <https://doi.org/10.1016/j.molliq.2018.01.188>.
- (2) Agarwal, S.; Tyagi, I.; Gupta, V. K.; Mashhadi, S.; Ghasemi, M. Kinetics and Thermodynamics of Malachite Green Dye Removal from Aqueous Phase Using Iron Nanoparticles Loaded on Ash. *J. Mol. Liq.* **2016**, *223*, 1340–1347. <https://doi.org/10.1016/j.molliq.2016.04.039>.
- (3) Garba, Z. N.; Lawan, I.; Zhou, W.; Zhang, M.; Yuan, Z.; Yuan, E. Z. Microcrystalline Cellulose (MCC) Based Materials as Emerging Adsorbents for the Removal of Dyes and Heavy Metals-A Review. *Sci. Total Environ.* **2019**, *717*, 135070. <https://doi.org/10.1016/j.scitotenv.2019.135070>.
- (4) Shi, Z.; Xu, C.; Guan, H.; Li, L.; Fan, L.; Wang, Y.; Liu, L.; Meng, Q.; Zhang, R. Magnetic Metal Organic Frameworks (MOFs) Composite for Removal of Lead and Malachite Green in Wastewater. *Colloids Surfaces A Physicochem. Eng. Asp.* **2018**, *539*, 382–390. <https://doi.org/10.1016/j.colsurfa.2017.12.043>.
- (5) Yadav, M.; Singh, G.; Jadeja, R. N. Phytoremediation for Heavy Metal Removal. In *Pollutants and Water Management*; Wiley Online Books; 2021; pp 128–150. <https://doi.org/https://doi.org/10.1002/9781119693635.ch6>.
- (6) Liu, L.; Gao, Z.; Su, X.; Chen, X.; Jiang, L.; Yao, J. Adsorption Removal of Dyes from Single and Binary Solutions Using a Cellulose-Based Bioadsorbent. *ACS Sustain. Chem. Eng.* **2015**, *3* (3), 432–442. <https://doi.org/10.1021/sc500848m>.
- (7) Gupta, V. K.; Agarwal, S.; Saleh, T. A. Synthesis and Characterization of Alumina-Coated Carbon Nanotubes and Their Application for Lead Removal. *J. Hazard. Mater.* **2011**, *185* (1), 17–23. <https://doi.org/10.1016/j.jhazmat.2010.08.053>.
- (8) Mittal, A.; Kaur, D.; Malviya, A.; Mittal, J.; Gupta, V. K. Adsorption Studies on the Removal of Coloring Agent Phenol Red from Wastewater Using Waste Materials as

- Adsorbents. *J. Colloid Interface Sci.* **2009**, *337* (2), 345–354. <https://doi.org/10.1016/j.jcis.2009.05.016>.
- (9) Yang, S. T.; Chen, S.; Chang, Y.; Cao, A.; Liu, Y.; Wang, H. Removal of Methylene Blue from Aqueous Solution by Graphene Oxide. *J. Colloid Interface Sci.* **2011**, *359* (1), 24–29. <https://doi.org/10.1016/j.jcis.2011.02.064>.
- (10) Hu, X. S.; Liang, R.; Sun, G. Super-Adsorbent Hydrogel for Removal of Methylene Blue Dye from Aqueous Solution. *J. Mater. Chem. A* **2018**, *6* (36), 17612–17624. <https://doi.org/10.1039/c8ta04722g>.
- (11) Li, D.; Li, Q.; Bai, N.; Dong, H.; Mao, D. One-Step Synthesis of Cationic Hydrogel for Efficient Dye Adsorption and Its Second Use for Emulsified Oil Separation. *ACS Sustain. Chem. Eng.* **2017**, *5* (6), 5598–5607. <https://doi.org/10.1021/acssuschemeng.7b01083>.
- (12) Han, H.; Wei, W.; Jiang, Z.; Lu, J.; Zhu, J.; Xie, J. Removal of Cationic Dyes from Aqueous Solution by Adsorption onto Hydrophobic/Hydrophilic Silica Aerogel. *Colloids Surfaces A Physicochem. Eng. Asp.* **2016**, *509*, 539–549. <https://doi.org/10.1016/j.colsurfa.2016.09.056>.
- (13) Saad, N.; Al-Mawla, M.; Moubarak, E.; Al-Ghoul, M.; El-Rassy, H. Surface-Functionalized Silica Aerogels and Alcohols for Methylene Blue Adsorption. *RSC Adv.* **2015**, *5* (8), 6111–6122. <https://doi.org/10.1039/c4ra15504a>.
- (14) Hong, Y.; Kim, J.; Choi, A.; Pal, M.; Lee, G. RSC Advances Highly Stable Mesoporous Silica Nanospheres Embedded with FeCo / Graphitic Shell Nanocrystals as Magnetically Recyclable Multifunctional Adsorbents for Wastewater Treatment †. *RSC Adv.* **2017**, *8*, 1089–1097. <https://doi.org/10.1039/C7RA12240C>.
- (15) Wu, X.; Hui, K. N.; Hui, K. S.; Lee, S. K.; Zhou, W.; Chen, R.; Hwang, D. H.; Cho, Y. R.; Son, Y. G. Adsorption of Basic Yellow 87 from Aqueous Solution onto Two Different Mesoporous Adsorbents. *Chem. Eng. J.* **2012**, *180*, 91–98. <https://doi.org/10.1016/j.cej.2011.11.009>.
- (16) Nekouei, F.; Nekouei, S.; Tyagi, I.; Gupta, V. K. Kinetic, Thermodynamic and Isotherm

- Studies for Acid Blue 129 Removal from Liquids Using Copper Oxide Nanoparticle-Modified Activated Carbon as a Novel Adsorbent. *J. Mol. Liq.* **2015**, *201*, 124–133. <https://doi.org/10.1016/j.molliq.2014.09.027>.
- (17) El-Zahhar, A. A.; Awwad, N. S.; El-Katori, E. E. Removal of Bromophenol Blue Dye from Industrial Waste Water by Synthesizing Polymer-Clay Composite. *J. Mol. Liq.* **2014**, *199*, 454–461. <https://doi.org/10.1016/j.molliq.2014.07.034>.
- (18) Ray, P. Z.; Shipley, H. J. Inorganic Nano-Adsorbents for the Removal of Heavy Metals and Arsenic: A Review. *RSC Adv.* **2015**, *5* (38), 29885–29907. <https://doi.org/10.1039/c5ra02714d>.
- (19) Valodkar, M.; Singh, P.; Jadeja, R. N.; Thounaojam, M.; Devkar, R.; Thakore, S. Cytotoxicity Evaluation and Antimicrobial Studies of Starch Capped Water Soluble Copper Nanoparticles. *J. Hazard. Mater.* **2012**, *202*, 244–249. <https://doi.org/10.1016/j.jhazmat.2011.11.077>.
- (20) Guleria, A.; Kumari, G.; Lima, E. C. Cellulose-g-Poly-(Acrylamide-Co-Acrylic Acid) Polymeric Bioadsorbent for the Removal of Toxic Inorganic Pollutants from Wastewaters. *Carbohydr. Polym.* **2020**, *228*, 115396. <https://doi.org/10.1016/j.carbpol.2019.115396>.
- (21) Mallampati, R.; Xuanjun, L.; Adin, A.; Valiyaveetil, S. Fruit Peels as Efficient Renewable Adsorbents for Removal of Dissolved Heavy Metals and Dyes from Water. *ACS Sustain. Chem. Eng.* **2015**, *3* (6), 1117–1124. <https://doi.org/10.1021/acssuschemeng.5b00207>.
- (22) Saha, G. C.; Hoque, I. U.; Al, M.; Miah, M.; Holze, R.; Chowdhury, D. A.; Khandaker, S.; Chowdhury, S. Biosorptive Removal of Lead from Aqueous Solutions onto Taro (Colocasia esculenta (L.) Schott) as a Low Cost Bioadsorbent: Characterization, Equilibria, and Kinetics. *Biochem. Pharmacol.* **2017**, *5*, 2151–2162. <https://doi.org/10.1016/j.jece.2017.04.013>.
- (23) Cao, Y.; Xiao, W.; Shen, G.; Ji, G.; Zhang, Y.; Gao, C.; Han, L. Carbonization and Ball Milling on the Enhancement of Pb(II) Adsorption by Wheat Straw: Competitive Effects of Ion Exchange and Precipitation. *Bioresour. Technol.* **2019**, *273*, 70–76.

- <https://doi.org/10.1016/j.biortech.2018.10.065>.
- (24) Lima, J. P.; Alvarenga, G.; Goszczynski, A. C. F.; Rosa, G. R.; Lopes, T. J. Batch Adsorption of Methylene Blue Dye Using *Enterolobium Contortisiliquum* as Bioadsorbent : Experimental , Mathematical Modeling and Simulation. *J. Ind. Eng. Chem.* **2020**, *91*, 362–371. <https://doi.org/10.1016/j.jiec.2020.08.029>.
- (25) Jiang, R.; Tian, J.; Zheng, H.; Qi, J.; Sun, S.; Li, X. A Novel Magnetic Adsorbent Based on Waste Litchi Peels for Removing Pb (II) from Aqueous Solution. *J. Environ. Manage.* **2015**, *155*, 24–30. <https://doi.org/10.1016/j.jenvman.2015.03.009>.
- (26) Ebadi, A.; Rafati, A. A. Preparation of Silica Mesoporous Nanoparticles Functionalized with β -Cyclodextrin and Its Application for Methylene Blue Removal. *J. Mol. Liq.* **2015**, *209* (1), 239–245. <https://doi.org/10.1016/j.molliq.2015.06.009>.
- (27) Munagapati, V. S.; Kim, D. S. Adsorption of Anionic Azo Dye Congo Red from Aqueous Solution by Cationic Modified Orange Peel Powder. *J. Mol. Liq.* **2016**, *220*, 540–548. <https://doi.org/10.1016/j.molliq.2016.04.119>.
- (28) Das, M.; Yadav, M.; Shukla, F.; Ansari, S.; Jadeja, R. N.; Thakore, S. Facile Design of a Dextran Derived Polyurethane Hydrogel and Metallopolymer: A Sustainable Approach for Elimination of Organic Dyes and Reduction of Nitrophenols. *New J. Chem.* **2020**, *44* (44), 19122–19134. <https://doi.org/10.1039/d0nj01871f>.
- (29) Kedzierska-Matyssek, M.; Matwijczuk, A.; Florek, M.; Barlowska, J.; Wolanciuk, A.; Matwijczuk, A.; Chrusciel, E.; Walkowiak, R.; Karcz, D.; Gladyszewska, B. Application of FTIR Spectroscopy for Analysis of the Quality of Honey. In *Contemporary Research Trends in Agricultural Engineering*; 2018; Vol. 10, pp 1–8.
- (30) Chen, X.; Liu, L.; Luo, Z.; Shen, J.; Ni, Q.; Yao, J. Facile Preparation of a Cellulose-Based Bioadsorbent Modified by HPEI in Heterogeneous System for High-efficiency Removal of Multiple Types of Dyes. *React. Funct. Polym.* **2018**, *125*, 77–83. <https://doi.org/10.1016/j.reactfunctpolym.2018.02.009>.
- (31) Teshale, F.; Karthikeyan, R.; Sahu, O. Synthesized Bioadsorbent from Fish Scale for

- Chromium (III) Removal. *Micron* **2020**, *130*, 102817.
<https://doi.org/10.1016/j.micron.2019.102817>.
- (32) Herrera-Barros, A.; Bitar-Catro, N.; Villabona-Ortiz, A.; Tejada-Tovar, C.; Gonzalez-Delgado, A. D. Nickel Adsorption from Aqueous Solution Using Lemon Peel Biomass Chemically Modified with TiO₂ Nanoparticles. *Sustain. Chem. Pharm.* **2020**, *17*, 100299.
<https://doi.org/10.1016/j.scp.2020.100299>.
- (33) Huang, Q.; Hu, D.; Chen, M.; Bao, C.; Jin, X. Sequential Removal of Aniline and Heavy Metal Ions by Jute Fiber Biosorbents: A Practical Design of Modifying Adsorbent with Reactive Adsorbate. *J. Mol. Liq.* **2019**, *285*, 288–298.
<https://doi.org/10.1016/j.molliq.2019.04.115>.
- (34) Aichour, A.; Zaghouane-boudiaf, H. Single and Competitive Adsorption Studies of Two Cationic Dyes from Aqueous Mediums onto Cellulose-Based Modified Citrus Peels/Calcium Alginate Composite. *Int. J. Biol. Macromol.* **2020**, *154*, 1227–1236.
<https://doi.org/10.1016/j.ijbiomac.2019.10.277>.
- (35) Feng, Y.; Liu, Y.; Xue, L.; Sun, H.; Guo, Z.; Zhang, Y.; Yang, L. Carboxylic Acid Functionalized Sesame Straw: A Sustainable Cost-Effective Bioadsorbent with Superior Dye Adsorption Capacity. *Bioresour. Technol.* **2017**, *238* (50), 675–683.
<https://doi.org/10.1016/j.biortech.2017.04.066>.
- (36) Li, R.; Liang, W.; Wang, J. J.; Gaston, L. A.; Huang, D.; Huang, H.; Lei, S.; Kumar, M.; Zhou, B.; Xiao, R.; et al. Facilitative Capture of As (V), Pb (II) and Methylene Blue from Aqueous Solutions with MgO Hybrid Sponge-like Carbonaceous Composite Derived from Sugarcane Leafy Trash. *J. Environ. Manage.* **2018**, *212*, 77–87.
<https://doi.org/10.1016/j.jenvman.2017.12.034>.
- (37) Feng, Y.; Zhou, H.; Liu, G.; Qiao, J.; Wang, J.; Lu, H.; Yang, L.; Wu, Y. Methylene Blue Adsorption onto Swede Rape Straw (*Brassica Napus* L.) Modified by Tartaric Acid: Equilibrium, Kinetic and Adsorption Mechanisms. *Bioresour. Technol.* **2012**, *125*, 138–144. <https://doi.org/10.1016/j.biortech.2012.08.128>.
- (38) Edathil, A. A.; Shittu, I.; Hisham Zain, J.; Banat, F.; Haija, M. A. Novel Magnetic Coffee

- Waste Nanocomposite as Effective Bioadsorbent for Pb(II) Removal from Aqueous Solutions. *J. Environ. Chem. Eng.* **2018**, *6* (2), 2390–2400. <https://doi.org/10.1016/j.jece.2018.03.041>.
- (39) Jalil, A. A.; Triwahyono, S.; Yaakob, M. R.; Azmi, Z. Z. A.; Sapawe, N.; Kamarudin, N. H. N.; Setiabudi, H. D.; Jaafar, N. F.; Sidik, S. M.; Adam, S. H.; et al. Utilization of Bivalve Shell-Treated Zea Mays L. (Maize) Husk Leaf as a Low-Cost Biosorbent for Enhanced Adsorption of Malachite Green. *Bioresour. Technol.* **2012**, *120*, 218–224. <https://doi.org/10.1016/j.biortech.2012.06.066>.
- (40) Qi, X.; Wei, W.; Su, T.; Zhang, J.; Dong, W. Fabrication of a New Polysaccharide-Based Adsorbent for Water Purification. *Carbohydr. Polym.* **2018**, *195*, 368–377. <https://doi.org/10.1016/j.carbpol.2018.04.112>.
- (41) Subbaiah, V.; Wen, J.; Pan, C.; Gutha, Y.; Wen, J. Enhanced Adsorption Performance of Reactive Red 120 Azo Dye from Aqueous Solution Using Quaternary Amine Modified Orange Peel Powder. *J. Mol. Liq.* **2019**, *285*, 375–385. <https://doi.org/10.1016/j.molliq.2019.04.081>.
- (42) Lee, S. Y.; Choi, H. J. Persimmon Leaf Bio-Waste for Adsorptive Removal of Heavy Metals from Aqueous Solution. *J. Environ. Manage.* **2018**, *209*, 382–392. <https://doi.org/10.1016/j.jenvman.2017.12.080>.
- (43) Nawaz, H.; Zaman, Q.; Kausar, A.; Noreen, S.; Iqbal, M. Efficient Remediation of Zr (IV) Using Citrus Peel Waste Biomass : Kinetic , Equilibrium and Thermodynamic Studies. *Ecol. Eng.* **2016**, *95*, 216–228. <https://doi.org/10.1016/j.ecoleng.2016.06.087>.
- (44) Hu, C.; Zhu, P.; Cai, M.; Hu, H.; Fu, Q. Comparative Adsorption of Pb(II), Cu(II) and Cd(II) on Chitosan Saturated Montmorillonite: Kinetic, Thermodynamic and Equilibrium Studies. *Appl. Clay Sci.* **2017**, *143*, 320–326. <https://doi.org/10.1016/j.clay.2017.04.005>.
- (45) Maruthapandi, M.; Kumar, V. B.; Luong, J. H. T.; Gedanken, A. Kinetics , Isotherm , and Thermodynamic Studies of Methylene Blue Adsorption on Polyaniline and Polypyrrole Macro – Nanoparticles Synthesized by C - Dot-Initiated Polymerization. *ACS Omega*

- 2018**, 3, 7196–7203. <https://doi.org/10.1021/acsomega.8b00478>.
- (46) Yadav, M.; Das, M.; Savani, C.; Thakore, S.; Jadeja, R. Maleic Anhydride Cross-Linked β -Cyclodextrin-Conjugated Magnetic Nanoadsorbent: An Ecofriendly Approach for Simultaneous Adsorption of Hydrophilic and Hydrophobic Dyes. *ACS Omega* **2019**, 4, 11993–12003. <https://doi.org/10.1021/acsomega.9b00881>.
- (47) Das, S.; Dash, S. K.; Parida, K. M. Kinetics, Isotherm, and Thermodynamic Study for Ultrafast Adsorption of Azo Dye by an Efficient Sorbent: Ternary Mg/(Al + Fe) Layered Double Hydroxides. *ACS Omega* **2018**, 3, 2532–2545. <https://doi.org/10.1021/acsomega.7b01807>.
- (48) Ren, H.; Kulkarni, D. D.; Kodiyath, R.; Xu, W.; Choi, I. Competitive Adsorption of Dopamine and Rhodamine 6G on the Surface of Graphene Oxide. *Appl. Mater. Interfaces* **2014**, 6, 2459–2470.
- (49) Zhao, F.; Repo, E.; Yin, D.; Meng, Y.; Jafari, S.; Sillanpaa, M. EDTA-Cross-Linked β -Cyclodextrin: An Environmentally Friendly Bifunctional Adsorbent for Simultaneous Adsorption of Metals and Cationic. *Environ. Sci. Technol.* **2015**, 49 (17), 10570–10580.
- (50) Feng, N.; Guo, X.; Liang, S.; Zhu, Y.; Liu, J. Biosorption of Heavy Metals from Aqueous Solutions by Chemically Modified Orange Peel. *J. Hazard. Mater.* **2011**, 185 (1), 49–54. <https://doi.org/10.1016/j.jhazmat.2010.08.114>.
- (51) Yu, J. X.; Chi, R. A.; Guo, J.; Zhang, Y. F.; Xu, Z. G.; Xiao, C. Q. Desorption and Photodegradation of Methylene Blue from Modified Sugarcane Bagasse Surface by Acid TiO₂hydrosol. *Appl. Surf. Sci.* **2012**, 258 (8), 4085–4090. <https://doi.org/10.1016/j.apsusc.2011.12.106>.
- (52) Zhou, Y.; Cao, S.; Xi, C.; Li, X.; Zhang, L.; Wang, G.; Chen, Z. A Novel Fe₃O₄/Graphene Oxide/Citrus Peel-Derived Bio-Char Based Nanocomposite with Enhanced Adsorption Affinity and Sensitivity of Ciprofloxacin and Sparfloxacin. *Bioresour. Technol.* **2019**, 292, 121951. <https://doi.org/10.1016/j.biortech.2019.121951>.
- (53) Oualid, H. A.; Abdellaoui, Y.; Laabd, M.; Ouardi, M. El; Brahmi, Y.; Iazza, M.; Oualid, J.

- A. Eco-Efficient Green Seaweed *Codium Decorticatum* Biosorbent for Textile Dyes : Characterization , Mechanism , Recyclability , and RSM Optimization. *ACS Omega* **2020**, *5*, 22192–22207. <https://doi.org/10.1021/acsomega.0c02311>.
- (54) Jin, X.; Xiang, Z.; Liu, Q.; Chen, Y.; Lu, F. Polyethyleneimine-Bacterial Cellulose Bioadsorbent for Effective Removal of Copper and Lead Ions from Aqueous Solution. *Bioresour. Technol.* **2017**, *244*, 844–849. <https://doi.org/10.1016/j.biortech.2017.08.072>.
- (55) Khoshsang, H.; Ghaffarinejad, A. Rapid Removal of Lead (II) Ions from Aqueous Solutions by Saffron Flower Waste as a Green Biosorbent. *J. Environ. Chem. Eng.* **2018**, *6* (5), 6021–6027. <https://doi.org/10.1016/j.jece.2018.09.020>.
- (56) Herald, E.; Lestari, W. W.; Permatasari, D.; Arimurti, D. D. Biosorbent from Tomato Waste and Apple Juice Residue for Lead Removal. *J. Environ. Chem. Eng.* **2018**, *6* (1), 1201–1208. <https://doi.org/10.1016/j.jece.2017.12.026>.
- (57) Menezes, J. M. C.; da Silva Bento, A. M.; da Silva, J. H.; de Paula Filho, F. J.; da Costa, J. G. M.; Coutinho, H. D. M.; Pereira Teixeira, R. N. Equilibrium, Kinetics and Thermodynamics of Lead (II) Adsorption in Bioadsorbent Composed by *Caryocar Coriaceum* Wittm Barks. *Chemosphere* **2020**, *261*, 128144. <https://doi.org/10.1016/j.chemosphere.2020.128144>.
- (58) Guo, S.; Jiao, P.; Dan, Z.; Duan, N.; Zhang, J.; Chen, G.; Gao, W. Synthesis of Magnetic Bioadsorbent for Adsorption of Zn(II), Cd(II) and Pb(II) Ions from Aqueous Solution. *Chem. Eng. Res. Des.* **2017**, *126*, 217–231. <https://doi.org/10.1016/j.cherd.2017.08.025>.
- (59) Somsesta, N.; Sricharoenchaikul, V.; Aht-Ong, D. Adsorption Removal of Methylene Blue onto Activated Carbon/Cellulose Biocomposite Films: Equilibrium and Kinetic Studies. *Mater. Chem. Phys.* **2020**, *240*, 122221. <https://doi.org/10.1016/j.matchemphys.2019.122221>.
- (60) Allafchian, A.; Mousavi, Z. S.; Hosseini, S. S. Application of Cress Seed Mucilage Magnetic Nanocomposites for Removal of Methylene Blue Dye from Water. *Int. J. Biol. Macromol.* **2019**, *136*, 199–208. <https://doi.org/10.1016/j.ijbiomac.2019.06.083>.

- (61) Stavrinou, A.; Aggelopoulos, C. A.; Tsakiroglou, C. D. Exploring the Adsorption Mechanisms of Cationic and Anionic Dyes onto Agricultural Waste Peels of Banana , Cucumber and Potato : Adsorption Kinetics and Equilibrium Isotherms as a Tool. *J. Environ. Chem. Eng.* **2018**, *6*, 6958–6970. <https://doi.org/10.1016/j.jece.2018.10.063>.